Universidade de Aveiro
2019
Departamento de Engenharia de Materiais e Cerâmica

Flávia Daniela Santos Lopes

Bioengenharia de sistemas nano estruturados com base em superfícies inspiradas na natureza para regeneração de tecidos humanos

Bioengineering of nanostructured systems based on nature-inspired surfaces for regeneration of human tissues

Universidade de Aveiro
2019

Departamento de Engenharia de Materiais e Cerâmica

Flávia Daniela Santos Lopes

Bioengenharia de sistemas nano estruturados com base em superfícies inspiradas na natureza para regeneração de tecidos humanos

Bioengineering of nanostructured systems based on nature-inspired surfaces for regeneration of human tissues

Dissertação apresentada à Universidade de Aveiro para cumprimento dos requisitos necessários à obtenção do grau de Mestre em Materiais e Dispositivos Biomédicos, realizada sob a orientação científica da Doutora Sónia Gonçalves Patrício e da Doutora Maria Clara Rosa da Silva Correia Correia, Investigadoras Doutoradas (nível I) da Universidade de Aveiro e do Professor Doutor João Filipe Colardelle da Luz Mano, Professor Catedrático da Universidade de Aveiro.

o júri

presidente

Professor Doutor João André da Costa Tedim
Professor Auxiliar em Regime Laboral da Universidade de Aveiro

Doutora Carla Andreia Cunha Vilela
Investigadora Doutorada (nível I) da Universidade de Aveiro

Doutora Sónia Gonçalves Patrício
Investigadora Doutorada (nível I) da Universidade de Aveiro

agradecimentos

Em primeiro lugar, gostaria de expressar o meu agradecimento ao professor João Mano pela incrível oportunidade de integrar o grupo de investigação COMPASS. Em segundo, agradeço à Dra. Sónia Patrício, minha orientadora, e à Dra. Clara Correia, minha coorientadora, por toda a orientação e partilha de conhecimentos, bem como por toda a disponibilidade para o sucesso da realização desta tese. Quero agradecer a todos os que integram o grupo COMPASS, que de uma forma ou outra contribuíram para o desenvolvimento e conclusão deste trabalho.

Agradeço ainda a todos os amigos sempre presentes e às amizades construídas ao longo de todo o meu percurso académico, que ficaram para a vida, pela compreensão, paciência, apoio e pelas palavras de motivação.

Minha profunda e sincera gratidão às pessoas mais importantes da minha vida: os meus pais, irmão e namorado. Obrigado pai e mãe, meus pilares, a quem não tenho palavras suficientes para expressar tudo o que fazem por mim, pelo incansável apoio, motivação e por todos os sacrifícios feitos da vossa parte para me proporcionarem a conclusão deste curso. Obrigado por me permitirem ser quem sou hoje, por todos os ensinamentos partilhados e por me mostrarem a vossa força para superar todos os obstáculos da vida. Vocês são o meu maior modelo. Esta tese é dedicada especialmente a vocês.

palavras-chave

Biomimetismo, Superfícies superhidrofóbicas-superhidrofílicas, *Layer by-Layer,* Micro-membranas autónomas, Engenharia modular de tecidos

resumo

A engenharia modular de tecidos visa mimetizar a complexidade do tecido nativo com arquiteturas 3D bem definidas e interações sinérgicas de várias linhas celulares através da geração de unidades modulares funcionais repetidas que serão montadas em um tecido funcional. Esses blocos modulares devem exibir características microestruturais específicas para imitar a arquitetura complexa de tecidos nativos. Para a produção direta de unidades modulares, as superfícies superhidrofóbicas-superhidrofílicas (SH-SL) padronizadas surgiram como plataformas promissoras para uma fabricação escalável de unidades modulares à microescala para desenvolver tecidos funcionais projetados pela abordagem *bottom-up*. Neste sentido, e inspirado no efeito de *Lotus*, o presente trabalho visa a produção de micro-membranas autónomas estratificadas baseadas nos biopolímeros poli-l-lisina (PLL) e alginato (ALG) através da metodologia *Layer-by-Layer (LbL)*. Para este propósito, inicialmente foram desenvolvidas superfícies SH-SL padronizadas à microescala com diferentes formas geométricas. Posteriormente, hidrogéis de alginato foram formados *in situ* pelo método *standing droplet* nas áreas SL que serviram de template de sacrifício para a produção de membranas autónomas pela deposição sequencial dos polieletrólitos através de interações electrostáticas. Relativamente às condições de deposição dos polímeros, na análise do potencial zeta verificaram-se as cargas de cada composto, enquanto que a microbalança de quartzo (QCM-D) evidenciou a interação eletrostática entre a PLL e o ALG. A análise por ATR-FTIR, confirmou a presença dos polímeros na membrana resultante. Após o destaque, as membranas forma reticuladas com genipina (GnP) para melhorar as propriedades mecânicas a fim de promover a adesão e proliferação celular. Ensaios biológicos *com human umbilical vein endotelial cells* (HUVECs) e *human adipose stem cells* (hASCs) evidenciaram que as membranas de $[PLL/ALG]_{100}$ reticuladas apresentam viabilidade celular.

Keywords

Biomimetic, Superhydrophobic-superhydrophilic surfaces, *Layer by-Layer,* Freestanding micro-membranes, Modular tissue engineering

abstract

Modular tissue engineering aims to mimic the complexity of native tissue with well-defined 3D architectures and synergistic interactions of various cell lines by generating repeated functional modular units that will be assembled into a functional tissue. These modular blocks should exhibit specific microstructural characteristics to mimic the complex architecture of native tissues. For the direct production of modular units, patterned superhydrophobic-superhydrophilic (SH-SL) surfaces have emerged as promising platforms for scalable manufacturing of microscale modular units to develop functional tissues designed by the bottom-up approach. In this sense, and inspired by the Lotus effect, the present work aims at the production of freestanding (FS) stratificated micromembranes based on poly-l-lysine (PLL) and alginate (ALG) biopolymers through the Layer-by-Layer (LbL) methodology. For this purpose, initially microscale SH-SL surfaces with different geometric shapes were developed. Subsequently, alginate hydrogels were formed in situ by the standing droplet method in the SL areas that served as a sacrificial template to the production of freestanding membranes by sequential deposition of electrolytes through electrostatic interactions. Regarding the deposition conditions of the polymers, in the zeta potential analysis, the charges of each compound were verified, while the quartz microbalance (QCM-D) showed the electrostatic interaction between PLL and ALG. ATR-FTIR analysis confirmed the presence of polymers in the resulting membrane. After detachment, the resulting membranes crosslinked with genipin (GnP) to improve mechanical properties to promote cell adhesion and proliferation. Biological assays with human umbilical vein endothelial cells (HUVECs) and human adipose stem cells (hASCs) showed that the crosslinked $[PLL / ALG]_{100}$ membranes show cellular viability.

Contents

List of Figures

List of Abbreviations and acronyms

3D	Three-dimensional
α-MEM	α-minimum essential medium
ALG	Sodium alginate
ALP	Alkaline phosphatase
ATR-FTIR	Attenuated Total Reflectance Fourier Transformed Infrared
CA	Water contact angle
CAH	Contact angle hysteresis
CVD	Chemical vapor deposition
DAPI	*4',6'*-diamidino-*2*-phenylindole
DI	Deionized water
DMA	Droplet microarray
DMPA	2,2-dimethoxy-2-phenylacetophenone
DNA	Deoxyribonucleic acid
DPBS	Dulbecco's phosphate buffered saline
ECM	Extracellular matrix
EDC	1-ethyl-3-(3-dimethylaminopropyl)carbodiimide
EDMA	ethylene dimethacrylate
EDS	Energy-dispersive X-ray spectroscopy
EDTA	Ethylenediaminetetraacetic acid
FS	Freestanding
GDL	D-(+)-gluconic acid δ-lactone
GnP	Genipin
hASCs	Human adipose-derived stem cells
HEMA	2-hydroxyethyl methacrylate
HUVECs	Human umbilical vein endothelial cells
LbL	Layer-by-Layer
LMA	Library microarray
Mw	Molecular weight
MSCs	Mesenchymal Stem Cells

MTS	*3*-(*4,5*-dimethylthiazol-*2*-yl)-*5*-(*3*-carboxymethoxyphenyl)-*2*-(*4*-sulphofenyl)-2H-tetrazolium
NHS	N-hydroxysuccinimide
PFDT	1H,1H,2H,2H-perfluoro-1-decanethiol
PLL	Poly-L-lysine
pNPP	p-nitrophenyl phosphate
QCM-D	Quartz-crystal microbalance with dissipation monitoring
Rpm	rotations per minute
RT	room temperature
SA	slide angle
SEM	scanning electron microscopy
SH	Superhydrophobic
SL	Superhydrophilic
TE	Tissue Engineering
UV	Ultraviolet

Chapter 1: State-of-the-Art

1.1. Introduction

The limited availability of tissue donors and complications related with immunosuppressive drugs have fostered the quest of alternative therapeutic strategies. **Tissue engineering** (TE) is been widely explored as a promising biomedical approach toward the development of engineered functional tissues, aiming to restore biological function or replace failing organs.[1–3] This interdisciplinary research field relies on the interplay of three components: scaffolds, cells and regulatory signals[3,4] – Figure 1.1. Scaffolds are an essential element of the tissue engineering triad, supporting cell adhesion and proliferation, thus enabling the formation of a functional tissue.[3,5] In order to mimic the natural complexity of human tissues, scaffolds can be combined with different cell types and regulatory signals like growth factors and mechanical stimuli.

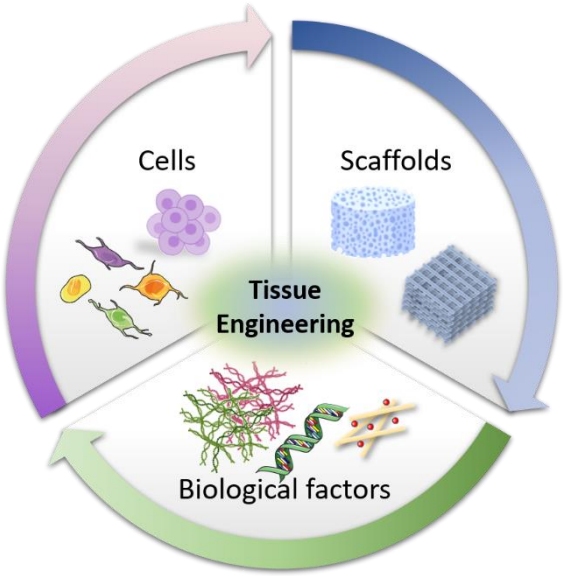

Figure 1.1 – Tissue engineering (TE) triad. The interplay of scaffolds, cells and biological factors allows the production of novel biomaterials for TE applications. Adapted from [4].

Traditional tissue engineering strategy employs a **top-down** approach (also known as **scaffold-directed**), in which bulk scaffolds are developed as a temporary support for cell attachment and proliferation. Hence, scaffold surface is enriched with functional cells that are then expected to populate all the scaffold and produce appropriate extracellular matrix (ECM) to restore or regenerate defective tissues.[6,7] However, macroscale scaffolds present difficult control of cell density, non-uniform cell distribution, vascularization and inadequate mass transport (oxygen diffusion, nutrients and growth factors) owing to the limited access to the internal scaffold. Different attempts have been made to overcome cell survival in thick tissue-like constructs (> 200 μm), including flow perfusion and

mechanical stimulation. Nevertheless, top down strategy is still too reductionist to recreate the complex microstructural organization of native tissues like vasculature, neuronal networks, or hexagonal lobules in the liver.[7]

Bottom-up, also known as **modular** approach has emerged as a promising alternative to eliminate the shortcomings of the conventional scaffolds from top-down approach. Bottom-up approach focuses on the fabrication of functional building blocks with organized microstructures that could promote cell guidance, extensive vascularization, adhesion, and eventual differentiation.[6,8] The building block functionality is provided by the heterogeneous assembly of distinct modular units (peptides, cells, and cell-encapsulating microgels) in a multiscale fashion.[9] Ultimately, these functional modular units can be assembly into large biological tissue-like constructs (Figure 1.2), mimicking the hierarchical architecture of native tissues.[7]

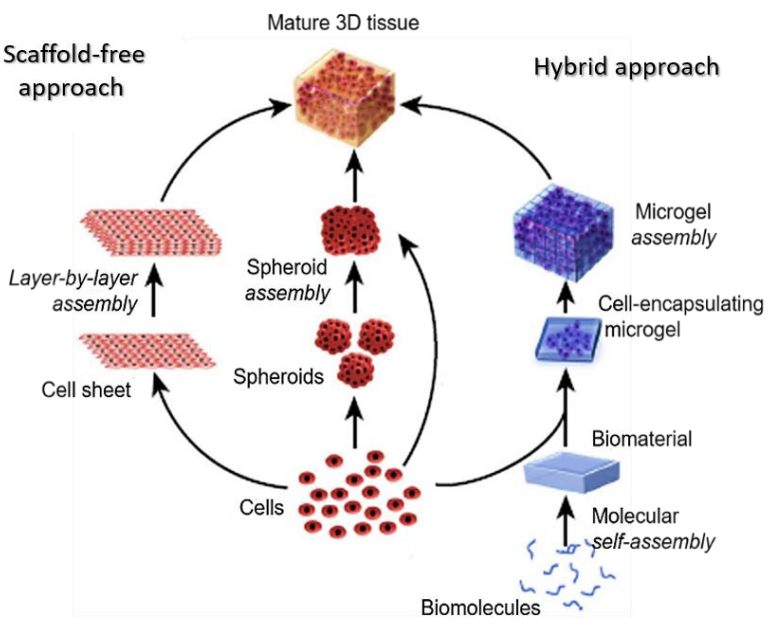

Figure 1.2 – Schematic of multiscale assembly strategies from bottom to top for engineering 3D tissue constructs. Adapted from [9].

Current bottom-up strategy relies on different technological approaches. One of them is based on the assembly of multicellular building blocks such as cell sheets and spheroids – **scaffold-free** TE approach. **Cell sheets** are conventionally prepared by culturing a monolayer of cells in petri dishes coated with a thermoresponsive polymer for cell sheet detachment. Currently, other responsive platforms (light, pH, electric and magnetic) have been exploited for cell sheet engineering.[10] These cell sheets can be then stacked layer-by-layer to build complex tissue structures like native vascular smooth muscle.[11] Such strategy offers the possibility to assembly layers from different cell types, enabling tissue

organization control toward the fabrication of hierarchical complex tissue engineered construct.

Spheroids are ball-shaped compacted cell aggregates that can be produced by different methodologies, ranging from antiadhesive cell-culture plates to microfluidic and hanging drop culture.[12,13] Interestingly, spheroids have self-assembling capacities for tissue fusion, thereby forming larger tissue constructs. Furthermore, spheroids can be also assembled into close-packed tissue by bioprinting technology.[14,15] Major drawbacks of current scaffold-free bottom-up approach are related with the feeble mechanical properties of the cellular building blocks, leading to possible cell damage during their manipulation.[16]

In this sense, a **hybrid** bottom-up strategy, combining the mutually advantages of scaffold-directed (seeded cells from top down approach) and scaffold-free approaches, has been emerged (Figure 1.3).[16]

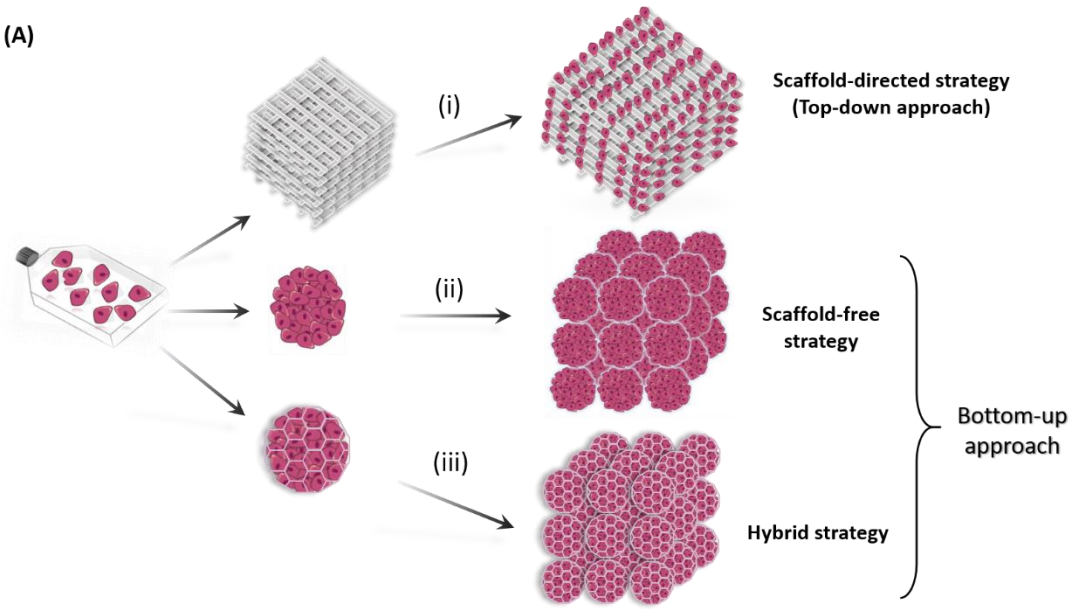

(B)

	Initial cell density	Mechanical properties	Funcionalization with biomolecules	Possibility of tissue self-assembly
Scaffold-directed	✗	✓	✗	✓
Scaffold-free	✓	✗	✓	✗
Hybrid	✓	✓	✓	✓

Figure 1.3 – Different technological tissue engineering approaches. (A) Expanded cells can be used (i) to seed onto scaffolds to produce tissue-engineered constructs (scaffold-directed or top down strategy); (ii) to produce spheroids to be latter assembled into scaffold-free constructs and (iii) to create spheroids within cage-like microscaffolds (hybrid approach). (B) Advantages and drawbacks of scaffold-directed, scaffold-free and hybrid TE approaches. Adapted from[16].

For instance, spheroids can be encapsulated into 3D robust micro-scaffolds creating mechanically robust tissue constructs, since mechanical properties of these constructs are dominated by the scaffold design and stiffness (Figure 1.3 Aiii). Moreover, as aforementioned, cells and biomaterials assemblies still allow additional functionalization of the heterogeneous building blocks with bioactive molecules (growth factors, enzymes, ECM molecules), affording the development of instructive and interactive "living" building blocks toward the engineering of macroscale biomimetic tissues.

1.2. Microfabrication Technology in bottom-up TE

Bottom-up or modular tissue engineering approach aims to engineer biomimetic tissue constructs by using heterogeneous building blocks with well-defined microarchitectural features. **Microfabrication** technology allows to create functional modular units at the microscale, with precise resolution control over the shape. Properties of modular biomaterials at such scales are significantly different from those at a macroscopic scale.[17] For this reason, microfabrication has been receiving much attention in recent years. Furthermore, microfabrication technology also provides advantages in terms of efficiency, reproducibility, cost-effectiveness and high miniaturization capacity.[18]

Several microfabrication techniques (Figure 1.4) have been employed for generating shape-controlled tissue modules, namely 3D bioprinting, microfluidic, electrospray, photolithography, micromolding and **superhydrophobic surfaces** (SH).[17,19–21]

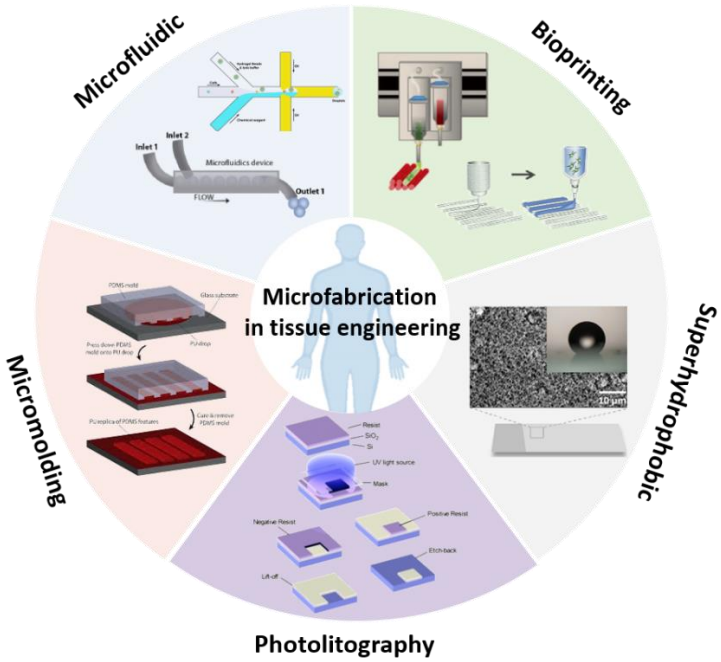

Figure 1.4 – Microfabrication techniques employed in tissue engineering bottom-up approach.

According to the scope of this master thesis, special attention will be dedicated to superhydrophobic surfaces as versatile platforms for the high-throughput fabrication of microscale scaffolding biomaterials with well-defined control over size and geometry.

1.3. Fundamentals of superhydrophobicity

Superhydrophobic (SH) surfaces exhibit an extremely high-water repellent behavior and are characterized by a water contact angle (CA) greater than 150° and, subsequently self-cleaning property. For a surface to be self-cleaning it is desirable for the liquid not only to not wet it, but also to be easily able to leave or slip off of the surface. The wettability is evaluated by the static and dynamic behavior of a liquid droplet over a solid surface. The contact angle is the angle formed by a liquid drop on the three-phase contact line on a flat material surface, which describe the static behavior. In order to characterize the dynamic performance, a parameter more relevant than the CA is the roll-off or sliding angle (SA), defined as the tilt required for the droplet to leave the surface. Related to this, it is the contact angle hysteresis (CAH), which is defined as the difference between advancing and receding CAs as the drop is moving, and the SA that is the inclination angle of the surface that cause the droplet to roll-off (see Figure 1.5). Thus, in addition to high CAs, these surfaces exhibit SA lower than 5° and CAH lower than 10°.[22–26]

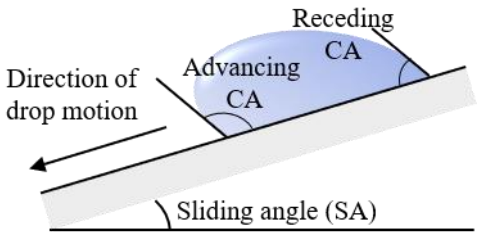

Figure 1.5 – Schematic representation of some of the relevant parameters to characterize slippery surfaces; tilt or sliding angle and advancing and receding contact angles. The contact angle hysteresis is the difference between advancing and receding angles. Adapted from[24].

Based on the numerical values of CA (θ), where they are measured using water as the liquid phase, and considering the wetting behaviour, the solid surfaces are generally classified into four different regimes. The surface is classified as (i) hydrophilic and (ii) hydrophobic if the CA is between 10° and 90° or if the CA is between 90° and 150°, respectively, being these the two most conventional regimes; (iii) superhydrophilic, if the CA is less than 10° and describes nearly perfect wetting; and in contrast, superhydrophobic if the CA is above 150° and describes a surface in a state of nearly perfect non-wetting, as shown in Figure 1.6.[24,27]

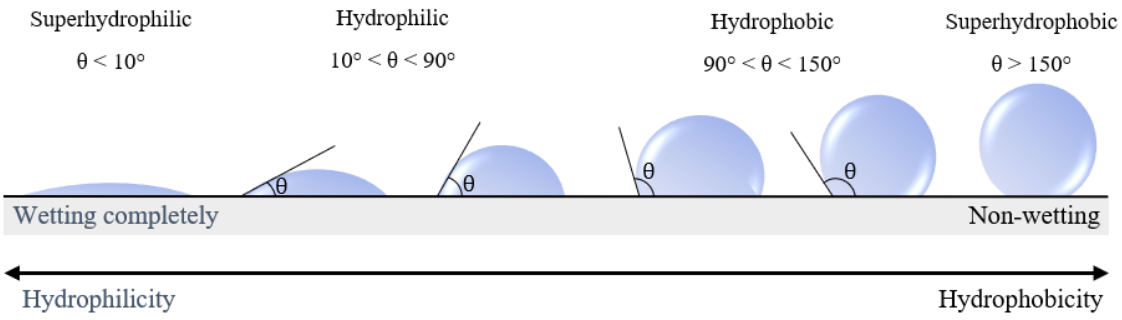

Figure 1.6 – Scheme of wetting behaviors of the solid surfaces. Adapted from[24,27].

Extensive interests of scientific community have been attracted to investigate bioinspired surfaces with special wettability because of the discoveries of unique wetting phenomena in nature, particularly in recent twenty years. For designing and controlling wettability features is crucial understanding the wetting phenomena of liquid (L) droplets on solid (S) surfaces.[28,29] The most fundamental theory about the wetting behaviours is the Young's model[30] for contact angle, θ_Y , of liquid droplets on smooth and chemically homogeneous solid surfaces (Figure 1.7 a) is described by equation,

$$\cos\theta_Y = \frac{\gamma_{SV} - \gamma_{SL}}{\gamma_{LV}} \qquad (Equation\ 1)$$

where γ_{SV}, γ_{SL} and γ_{LV} represent the interfacial tensions (energies, γ) of the solid-vapor, solid-liquid, and liquid-vapor, respectively.

The Young's wetting state does not consider the surface roughness of the solid surface assuming that the surface is perfectly smooth and flat as an ideal solid substrate and the CAs are normally based on the surface chemistry compositions or properties. However, solid surfaces inevitably have some surface textures in the real world.[28] Subsequently, in the 1940s, for the wetting of rough and heterogeneous solid surfaces, Cassie and Baxter[31] reporting the basis of superhydrophobicity, expanding on the work by Wenzel in 1936[32]. In the Cassie-Baxter wetting state[31] , liquid droplet rests on the surface asperities, given rise to air pockets at the liquid-solid (L-S) interface, as shown in Figure 1.7 b. As a result of the suspension of the water droplet on the asperities the CA, θ_{CB}, is the sum of all the contributions of the different phases given by following equation:

$$\cos\theta_{CB} = f_1\cos\theta_1 + f_2\cos\theta_2 \qquad (Equation\ 2)$$

where θ_1 and θ_2 are the CAs that liquid droplets make with solid surfaces 1 and 2; f_1 and f_2 ($f_1+f_2=1$) are the fractions of the phases 1 and 2 areas, respectively, on the surface below droplets.

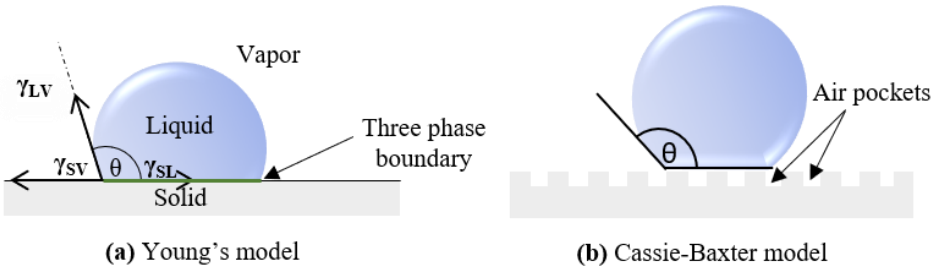

(a) Young's model **(b)** Cassie-Baxter model

Figure 1.7 – Schematic representations of the effect of surface structure on the wetting behavior of solid substrates. (a) A liquid droplet on an ideal flat substrate – Young's model. Diagram showing the forces at the three-phase contact line of a liquid droplet on a solid (b) Non-wetted behavior between the liquid and the rough substrate – Cassie-Baxter model. Adapted from [19].

Considering the wetting is not uniform and air packets do not let water to get into the surface cavities. In this case, water is in contact with solid and air packets, and water CA with air is equal to 180° and the equation above can be rewritten as:

$$\cos\theta_{CB} = f(1+\cos\theta) - 1 \qquad (Equation\ 3)$$

where the θ_{CB} is now a function of the fraction of solid (f) at the droplet interface and Young's CA of the solid (θ). The area fraction, *f*, is the ratio between the actual droplet contact area and the total surface area (Equation 4). This minimized liquid-surface contact area in that $f \to 0$ and the θ_{CB} approaches 180° results in SH surfaces exhibiting self-cleaning and water-repellent features.[33]

$$f = \frac{surface\ area\ wetted\ by\ liquid}{planar\ area\ below\ the\ droplet} \qquad (Equation\ 4)$$

Besides CA, CAH and SA, there are two others important parameters for achieve SH substrates: surface energy and surface morphology. Chemical compositions determine the surface energy and, when surface energy is lowered hydrophobicity is enhanced. On the other hand, the surface morphology may own hierarchical structures at micro- and/or nano-scale achieving superhydrophobicity.[34] So, the surface morphology is also equally important for obtaining superhydrophobicity being it is possible to achieve robust SH surfaces from hydrophilic surfaces by the appropriate roughness (Figure 1.8) and low

surface energy materials if the surface is able to stabilize the Cassie-Baxter wetting state.[24]

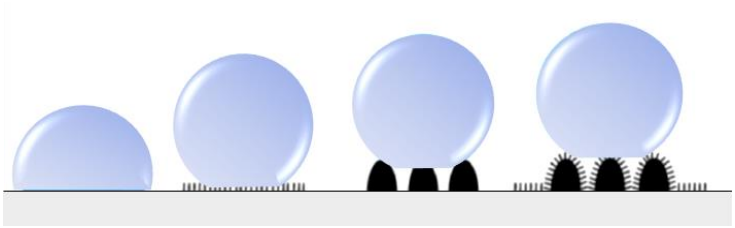

Figure 1.8 – Schematic of wetting behavior of different hydrophobic structures. Adapted from [24].

1.3.1. Superhydrophobic properties in nature

Many surfaces found in nature exhibit highly hydrophobic and self-cleaning properties. The most famous example of natural superhydrophobic surfaces are lotus leaves (*Nelumbo nucifera*). Several other plants also exhibit superhydrophobicity, including banana tree leaves, rice leaves, and red rose petals. Superhydrophobic properties are still found in animal surfaces like on the wings of cicada and butterflies, shark skin and mosquito eyes (Figure 1.9).[35,36]

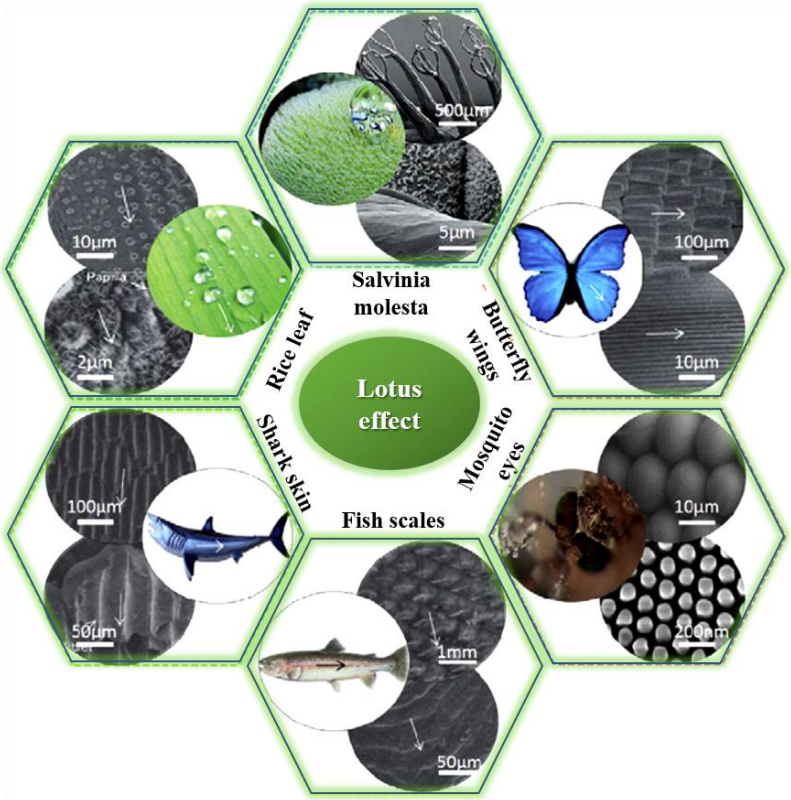

Figure 1.9 – The self-cleaning surfaces in Nature and respective SEM images. Adapted from [35].

The extreme water repellent behavior displayed by lotus leaves has led to the fabrication of the highest number of of biomimetic synthetic SH surfaces. On the lotus leaf, spherical water drops easily rolling off the leaf surface, carrying with them dust and dirt particles. The "**Lotus effect**" was coined by Barthlott [37] and Neinhuis [38] in the early 1997. For the first time, these researchers have observed the dual micro/nanostructure features of the lotus leaves by scanning electron (SEM) (see Figure 1.10 a and b). At the microscale, the leaf contains papillose epidermal cells with sizes between 5-10 µm (Figure 1.10 c) that are uniformly covered by epicuticular wax crystals (fine branch-like) of approximately 150 nm (Figure 1.10 d). [39] Therefore, self-cleaning properties (ability to remove dust and particles by moving water droplets) are the consequence of the dual (micro/nano) surface structures.

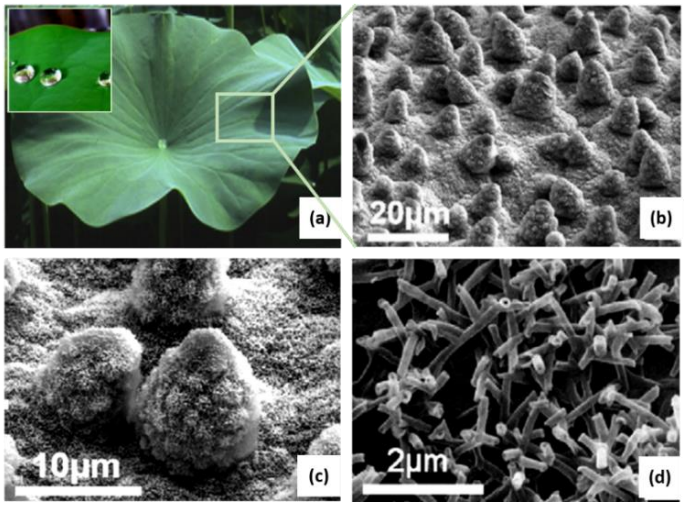

Figure 1.10 – (a) Image of a superhydrophobic lotus leaf (Nelumbo nucifera) and (b) corresponding SEM image of the leaf's surface; (c) micro- and (d) nano-structures of Lotus leaf. Adapted from [40,41].

The natural self-cleaning property have inspired the development of superhydrophobic surfaces for a plethora industrial and technological applications such as anti-corrosion coatings, anti-icing coatings, liquid-repellent textiles, oil/water separation, nanoparticles assembly, microfluidic devices, printing techniques, optical devices, high-sensitive sensors or batteries.[24,42,43]

Fabrication of super-hydrophobic surfaces usually requires the roughening of surface to get micro-nanostructures followed by surface modification, which leads to low surface energy. Various technique have been reported in the literature for the fabrication of superhydrophobic surfaces such as chemical vapor deposition (CVD)[44,45], aerosol-assisted CVD[46], phase separation[47], plasma treatment[48], chemical/electrochemical etching[49,50], electrospinning[51], electrodeposition[52], cold-spray technique[53], spray

coating methods[54] and so on[55,56]. Simplicity, less time consumption, cost-effectiveness and versatility are the important parameters during fabrication process. Moreover, characteristics like durability, corrosion resistance and storability of superhydrophobic surfaces are achieved at different levels, according to the employed fabrication methodology.

1.3.2. Superhydrophobic surfaces for biomedical applications

In 2000, Jiang and co-workers defined superamphiphobicity as an effect where surface roughness and surface chemistry combine to generate surfaces which are both SH and superoleophobic. This means that such surfaces possess CA greater than 150° along with low CAH not only to repel water but also oils/organic liquids of low surface-tension.[40,57,58] Deng *et al.*[59] developed a transparent robust SH surface from candle soot method. A glass slide was kept above a paraffin candle flame allowing a soot deposit (Figure 1.11), which is then coated with a thick silica shell through chemical vapor deposition. Afterwards, the hybrid carbon/silica network was coated with a semifluorinated silane by CVD forming a superamphiphobic surface.

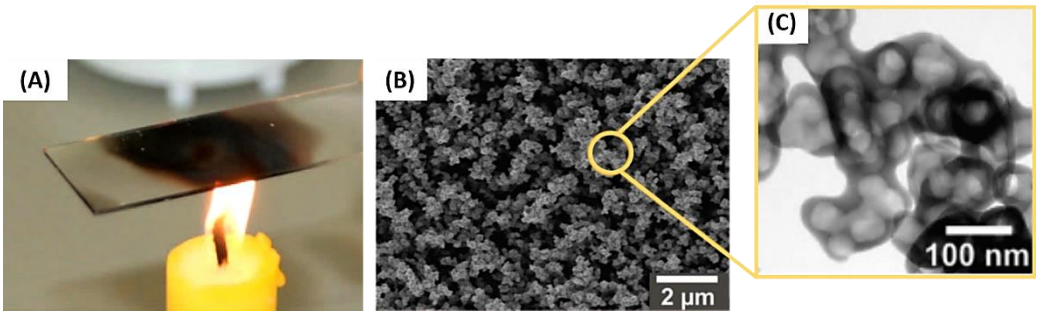

Figure 1.11 – Superhydrophobic surface from candle soot and morphology of porous structure. (A) Photograph depicting sample preparation. A Glass slide is held in the flame of a candle until a soot layer a few micrometers thick is deposited; (B) SEM image of the soot deposit after being coated with a silica shell; (C) High-resolution TEM image of a cluster after calcination, revealing the silica coating with holes that were previously filled with carbon particles. Adapted from[59].

This technology was employed for the production of individual polymeric microspheres and liquid-core capsules multi-layered under mild processing conditions.[60–63] For example, Costa et al. have developed a variety of multilayered and hierarchical capsules via assembly of polymeric droplets induced by superamphiphobic surfaces. These highly repellent substrates allowed an easy and precise control over the particle size and shape by simply tuning the dispensed volume above the SH surface (Figure 1.12).

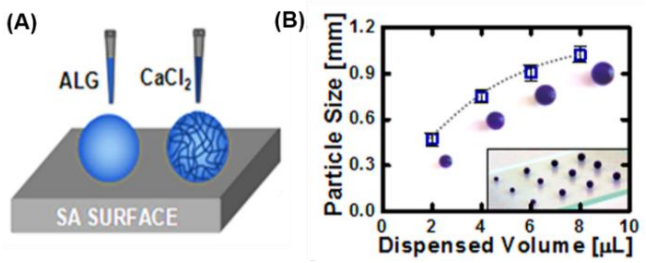

Figure 1.12 – (A) Spherical ALG droplet induced by a SA surface and their subsequent ionic gelation and (B) Effect of the dispensed volume of ALG solution on the size of the obtained hydrogel particles. Adapted from [61].

Another recent work relies on the use of these superhydrophobic and superamphiphobic surfaces to produce spheroidal hydrogel particles with controlled deformation, upon compressive action along the z axis (Figure 1.13).[64] Such spheroids have shown improved viability of encapsulated cells due to enhanced nutrient diffusion to the core, and led to a significantly faster drug release rate from the polymer network owing to the high surface area to volume ratio compared to spherical-shaped hydrogels. Therefore, such spheroidal particles hold great potential for drug delivery by oral or rectal administration routes, where the size would not be a limitation.

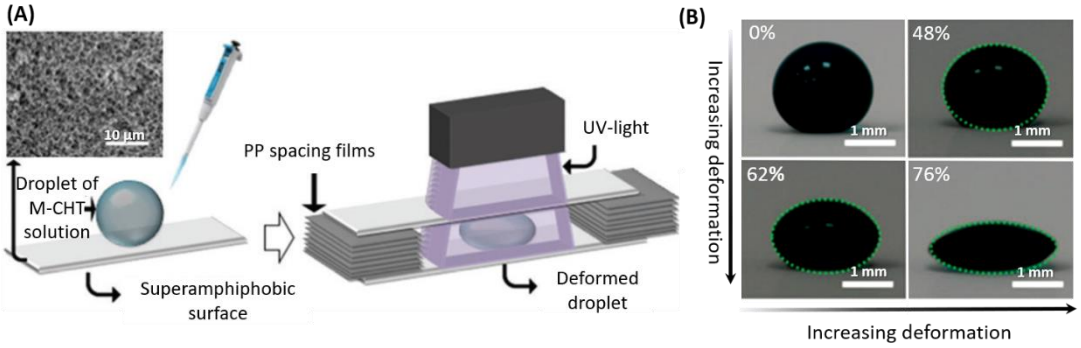

Figure 1.13 – (A) Schematic representation of the oblate spheroidal particle production method. Methacrylated chitosan (M-CHT) liquid precursor was squeezed between superamphiphobic surfaces separated using a known spacer height, followed by UV-crosslinking. (B) Spheroidal particle shape acquired upon removal of the upper superamphiphobic surface. Dotted green lines correspond to the yz plane representation of spheroids. Adapted from[64].

Generally, superhydrophobic surfaces are produced by tuning the chemistry or morphology of the material surfaces. For instance, apart from the candle soot method, rough superhydrophobic surfaces based on polystyrene were also developed by phase separation methods.[65–67] Recently, a non-textured superhydrophobic approach was developed to modulate wetting properties.[68] This new concept consisted on two dimensional (2D) molybdenum disulfide nanoassemblies, which have shown superhydrophobic behavior (CA > 150º) at a low degree of atomic defects, whereas superhydrophilic properties (CA ~ 0 º) were observed with high degree of atomic defects. The superhydrophobic MoS_2 could be coated on various substrates (glass, silica, rubber

and paper), thereby indicating high versatility for surface-coating applications. This study has still demonstrated the influence of the MoS_2 surface wetting characteristics cell-adhesion performance that can be leveraged for biomedical applications.

1.3.3. Patterned Superhydrophobic Surfaces – Droplet Microarrays

Superhydrophobic patterns consists on superhydrophobic surfaces with wettable superhydrophilic domains in specific locations. The combination of these extreme wetting properties on the same surface provide many advantages as exemplified in Figure 1.14: **A)** easy control of the geometry and position of liquid droplets; **B)** no requirement of surfactants to prefill micropatterns with aqueous solutions; **C)** utilization of superhydrophilic patterns as surface tension confined microchannels; **D)** close droplet position; **E)** controlling cell adhesion on superhydrophilic regions (within squares) and **F)** high-density microarrays of aqueous droplets by discontinuous dewetting.[69] This effect relies on the large difference in wettability between the superhydrophilic and superhydrophobic regions to passively dispense thousands of isolated droplets in the superhydrophilic spots with well-defined geometry and volume, referred as **droplet microarrays** (DMA). The rapid and facile droplet formation through discontinuous dewetting doesn't require multiple pipetting or a liquid handling device.

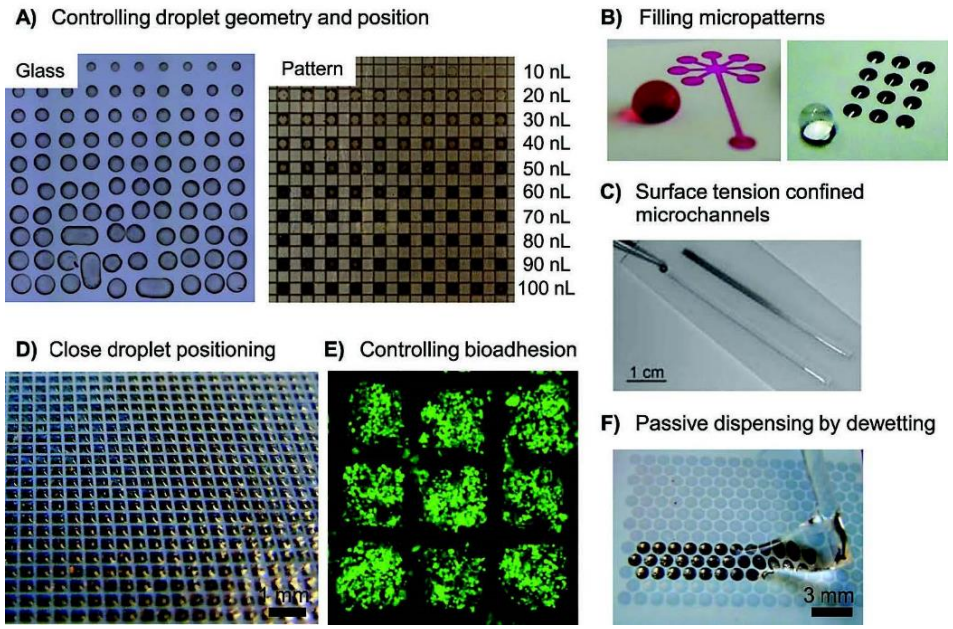

Figure 1.14 – Advantages of superhydrophobic-superhydrophilic patterns. Adapted from[69].

These microarrays can be used for the patterning of cells, chemicals, drugs, particles or any other components present in an aqueous solution. Therefore, DMA have become a valuable tool for **high-throughput** applications due to their miniaturized format, which requires fewer reagents, reducing significantly experimental costs. Each droplet can be regard as independent reservoir, and different cells and/or bioactive molecules can be encapsulated into these fully isolated compartments to perform biological reactions without cross-contamination. In this sense, numerous experimental assays can be realized in parallel, allowing expedite analysis procedures.

Currently, microarray technology is mostly employed for cell-based high-throughput screening of biochemical libraries for gene delivery, drug discovery, and toxicology. In complex assays of multicomponent experiments, different (bio)chemical agents require to be added into each individual microdroplet in DMA. Recently, Popova *et al.* developed a droplet microarray **"sandwiching" technology** to enable the single step addition of different (bio)chemicals into individual microdroplets on planar substrates (Figure 1.15 A).[70]

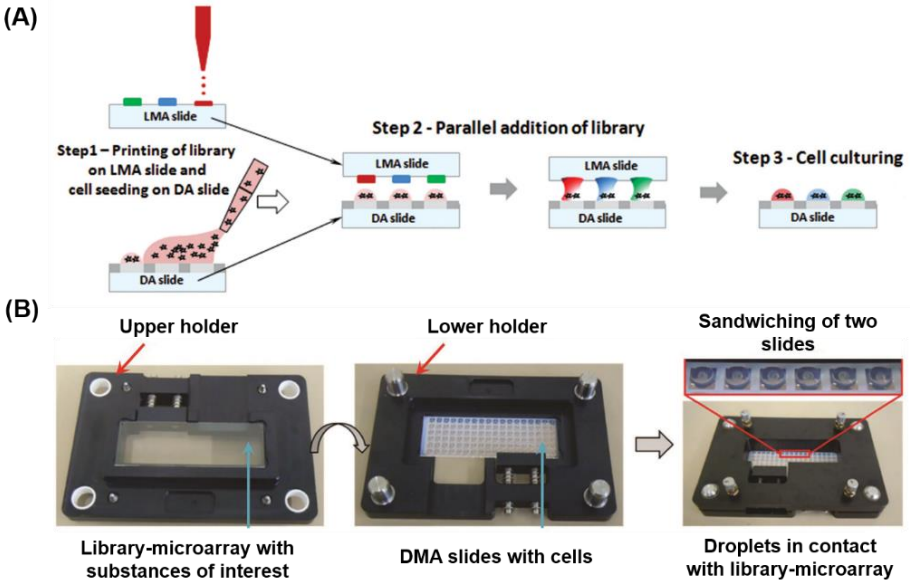

Figure 1.15 – (A) Schematic of a workflow of cell based screening using DMA sandwich chip and (B) Photographs of the handheld device used for aligning the droplets microarray when manipulating individual droplets using the sandwiching method. Adapted from[70,71].

First, a **library microarray** (LMA) slide was prepared by printing drugs or transfection mixtures onto a bare glass slide using a non-contact, ultralow volume dispenser in an array format corresponding to the pattern of the DMA slide. Precise alignment and "sandwiching" of the droplet microarray slide containing chemicals or cells with the library-microarray slide face-to-face leads to the dissolution of the

chemicals in the individual microdroplets after which the LMA was removed, without any cross-contamination between adjacent droplets, and the droplet microarray was cultured in medium.[72–74] The advantage of this method is that after preprinting a library-microarray using a conventional noncontact printer, the final addition of chemical libraries to the droplets can be done with a very simple handheld device (Figure 1.15 B).[71,75,76]

Recently, droplet microarray platform was also employed for full animal (e.g., zebrafish) high-throughput screenings.[77] Testing (bio)chemical compounds on whole organisms (in vivo screenings) is more physiologically relevant compared to cell culture models and can address complex processes such as behavior, pain, immunity, tumor metastasis, and vascularization that are out of reach for cell based assays. Single fish embryos were incorporated into microdroplet arrays by discontinuous dewetting (Figure 1.16) and parallel single-step pipetting-free addition of different fluorescently labeled peptoids was then performed by sandwiching technology to identify organ specificity. Each peptoid had a unique signature of tissue distribution in the larvae. Peptoids introduced into zebrafishes in DMA platforms were observed in the same organ locations as in in a 96-well plate, which requires one order magnitude higher peptoid amount. Therefore, the DMA technology can make whole organism screenings more cost- and time-efficient, as well as enable screenings that were not conducted before due to limited compound availability or complex handling.

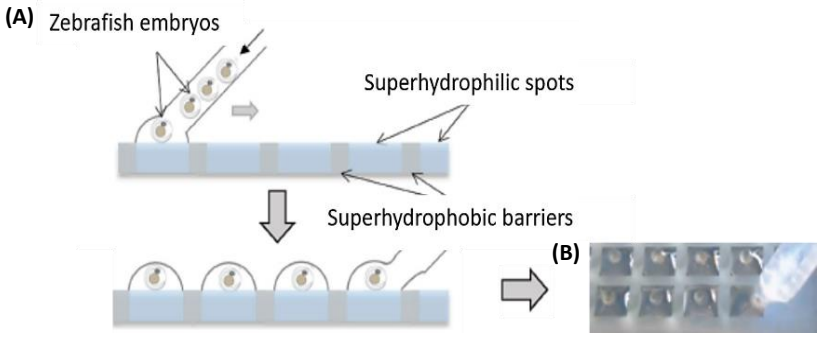

Figure 1.16 – Single collection of zebrafish embryos on Droplet-Microarray (DMA) platform. (A) Schematic representation and (B) image of the process of spreading zebrafish embryos using the effect of discontinuous dewetting. Adapted from[77].

Apart from cell- and animal-based high-throughput screening, droplet microarrays also enable the generation of miniaturized 3D hydrogel matrixes featuring individual complex cell microenvironments in a high-throughput manner. Bioactive molecules, non-

adherent cells and heterogeneous cell populations could be also encapsulated into the fully isolated hydrogel micropads for screening in 3D microenvironments. A recent work has reported a layer-by-layer organization of heterogeneous cells in a microgel by stacking a microgel array containing human umbilical vein endothelial cells with another layer containing fibroblast cells.[78] The ability to create arrays of hydrogel micropads encapsulating live cells in a simple and inexpensive way is important for enabling high-throughput screening of cells in physiologically relevant environments. It is important to emphasize that the hydrogel size depends on the size of hydrophilic spots.

Interestingly, hydrogel micropads can be also detached from DMA platform to form cell-laden microgels with different sizes and geometries (Figure 1.17).[79] In the same work, DMA platforms were also used to produce freestanding hydrogels loaded with functional magnetic particle, thereby enabling the use of magnetic field for the remote manipulation. The high-throughput fabrication of freestanding hydrogels with different shapes holds great potential for hybrid bottom-up tissue engineering approach.[80]

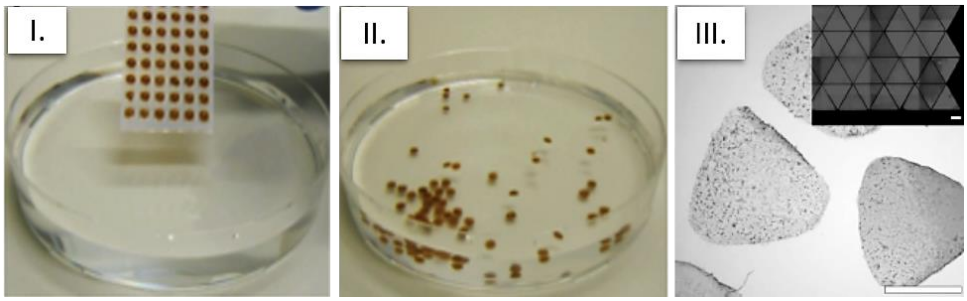

Figure 1.17 – (I) Array of square-shaped magnetic hydrogel particles (3 mm size length); (II) Freestanding hydrogel particles formed by immersing the array in buffer and (III) a microscopic image of FS hydrogel particles containing magnetic beads and arrays of fluorescent hydrogel particles anchored to the patterned surfaces. Adapted from[79].

Droplet microarrays still open up the possibility to carry out chemical synthesis in microdroplets, such as nanoparticles and metal–organic framework (MOF) microsheets.[81,82] Interestingly, MOF microsheets could be released from the substrate to generate freestanding MOF microsheets of defined geometries. This was achieved by first creating an array of copper acetate aqueous microdroplets with defined geometries through discontinuous dewetting. The well-defined shape of these droplets guided the nucleation and growth of MOFs along their 3D interfaces (Figure 1.18).

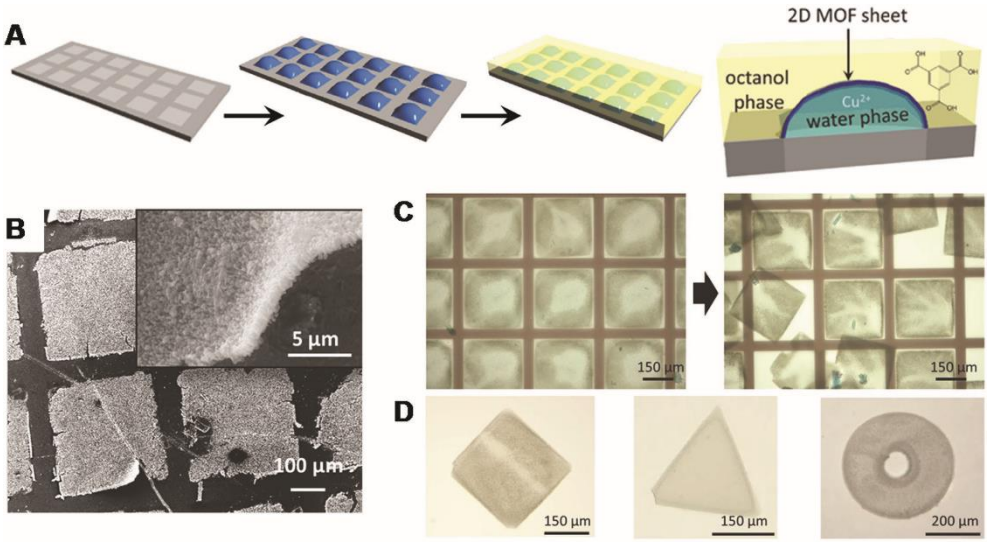

Figure 1.18 – (A) Schematic showing the formation of metal organic framework (MOF) microsheets at the spatially confined liquid–liquid interface between water droplet microarrays formed on a SL-SH micropatterned substrate and water immiscible octanol phase above the water droplets; (B) SEM images of patterned MOF superstructures; (C) Optical images showing the detachment of the MOF microsheets from the patterned substrate upon rinsing with ethanol. (D) Freestanding MOF superstructures with different shapes. Adapted from[82].

The ability to create arrays of droplets of various sizes and volumes from picoliters to microliters in precise locations on flat surfaces defines a revolutionary leap in technology for a plethora of biological applications, drug discovery, combinatorial synthesis, and personalized medicine. The reduced usage of sample and reagents, possibility for in situ analyses, higher sensitivity, and single-step formation of high-density droplet arrays allow DMA platforms to be suitable for point-of-care and diagnostics applications. These versatile platforms still open up new prospects towards sensor micro-ships and micro-reactors.[83]

1.4. Summary and outlook

Herein, we reviewed tissue engineering strategies mostly focused on building modular microtissues, in particular those ones that use cell/biomaterial combinations. A thorough analysis showed that such approaches enable to generating highly complex architectures with precise resolution control over shape and size, offering the possibility to mimic the the architectural micro-scale features of native niches (e.g. bifurcated vasculature, neuronal networks, or hexagonal lobules in the liver) which is particularly important for resulting physiological functionality. However, the scalability of theses complex 3D structures typically fail for most of these methods.

Among the various microfabrication techniques, superhydrophobic-superhydrophilic microarrays could emerged as promising platforms for a scalable manufacturing of modular microscale units toward the ultimate goal of creating biomimetic engineered tissues. These SH-SL microarrays provide accurate control over individual sizes, shapes, cell density, chemical concentrations and 3D spatial distribution of multiple components. The successful know-how on fabrication either stably anchored hydrogel microarrays or freestanding microgels with shape defined by the geometry of the hydrophilic array will soon allow extending this methodology towards novel freestanding micro-biomaterials.

References

[1] Zhang, L. G., Khademhosseini, A. & Webster, T. J. Tissue and Organ Regeneration. *Advances in Micro- and Nanotechnology*, Jenny Standford Publishing, New York, USA (2014).

[2] Khademhosseini, A. & Langer, R. A decade of progress in tissue engineering. *Nat. Protoc.* **11,** 1775–1781 (2016).

[3] O'Brien, F. J. Biomaterials & scaffolds for tissue engineering. *Mater. Today* **14,** 88–95 (2011).

[4] Costa, J. B., Pereira, H., Espregueira-Mendes, J., Khang, G., Oliveira, J. M., Reis, R. L. Tissue engineering in orthopaedic sports medicine : current concepts. *JISAKOS* **0,** 1–7 (2017).

[5] Smith, B. D. & Grande, D. A. The current state of scaffolds for musculoskeletal regenerative applications. *Nat. Rev. Rheumathology* **11**, 213–222 (2015).

[6] Tiruvannamalai-Annamalai, R., Armant, D. R. & Matthew, H. W. T. A Glycosaminoglycan Based, Modular Tissue Scaffold System for Rapid Assembly of Perfusable, High Cell Density, Engineered Tissues. *PLoS One* **9,** e84287 (2014).

[7] Nichol, J. W. & Khademhosseini, A. Modular tissue engineering: engineering biological tissues from the bottom up. *Soft Matter* **5,** 1312–1319 (2009).

[8] Lima, M. J., Pirraco, R. P., Sousa, R. A., Neves, N.M., Marques, A. P., Bhattacharya, M., Correlo, V. M., Reis, R. L. Bottom-up approach to construct microfabricated multi-layer scaffolds for bone tissue engineering. *Biomed. Microdevices* **16,** 69–78 (2014).

[9] Guven, S. *et al.* Multiscale assembly for tissue engineering and regenerative medicine. *Trends Biotechnol.* **33,** 269–279 (2015).

[10] Li, M., Ma, J., Gao, Y. & Yang, L. Cell sheet technology : a promising strategy in regenerative medicine. *Cytotherapy* **21,** 3–16 (2019).

[11] Williams, C., Xie, A. W., Yamato, M., Okano, T. & Wong, J. Y. Stacking of aligned cell sheets for layer-by-layer control of complex tissue structure. *Biomaterials* **32,** 5625–5632 (2011).

[12] Fennema, E., Rivron, N., Rouwkema, J., Blitterswijk, C. Van & Boer, J. De. Spheroid culture as a tool for creating 3D complex tissues. *Trends Biotechnol.* **31,** 108–115 (2013).

[13] Mehesz, A. N., Brown, J., Hajdu, Z., Beaver, W., Silva, J. V. L., Visconti, R. P., Markwald, R. R., Mironov, V. Scalable robotic biofabrication of tissue. *Biofabrication* **3,** 025002 (2011).

[14] Swaminathan, S., Hamid, Q., Sun, W. & Clyne, A. M. Bioprinting of 3D breast epithelial spheroids for human cancer models. *Biofabrication* **11,** 025003 (2019).

[15] Zhuang, P., Xuyang, A., An, J., Kai, C. & Yian, S. Biomaterials 3D neural tissue models: From spheroids to bioprinting. *Biomaterials* **154,** 113–133 (2018).

[16] Ovsianikov, A., Khademhosseini, A. & Mironov, V. The Synergy of Scaffold-Based and Scaffold-Free Tissue Engineering Strategies. *Trends Biotechnol.* **36,** 348–357 (2018).

[17] Cha, C., Piraino, F. & Khademhosseini, A. Microfabrication Technology in Tissue Engineering. *Tissue Engineering*, 283–310 (2015).

[18] Neto, A. I., Levkin, P. A. & Mano, J. F. Patterned superhydrophobic surfaces to process and characterize biomaterials and 3D cell culture. *Mater. Horizons* **5,** 379–393 (2018).

[19] Lima, A. C. & Mano, J. F. Micro /nano-structured superhydrophobic surfaces in the biomedical field: part I: basic concepts and biomimetic approaches. *Nanomedicine* **10,** 103–119 (2015).

[20] Ma, J. & Liu, J. Bioprinting of 3D tissues/organs combined with microfluidics. *RSC Adv.* **8,** 21712–21727 (2018).

[21] Correia, C. R., Reis, R. L. & Mano, J. F. Design Principles and Multifunctionality in Cell Encapsulation Systems for Tissue Regeneration. *Adv. Healthc. Mater.* **7,** 1701444 (2018).

[22] Yuan, Y. & Lee, T. R. Contact Angle and Wetting Properties. *Surface Science Techniques*, 3–34 (Springer Series in Surface Sciences 2013).

[23] Roach, P., Shirtcliffe, N. J., Newton, M. I., Newton, M. I. & Roach, P. Progress in

superhydrophobic surface development. *Soft Matter* **4,** 224–240 (2008).

[24] Jeevahan, J., Chandrasekaran, M., Joseph, G. B., Durairaj, R. B. & Mageshwaran, G. Superhydrophobic surfaces: a review on fundamentals, applications, and challenges. *J. Coatings Technol. Res.* **15,** 231–250 (2018).

[25] Avrămescu, R. E., Ghica, M. V., Dinu-Pîrvu, C., Prisada, R. & Popa, L. Superhydrophobic Natural and Artificial Surfaces – A Structural Approach. *Materials* **11,** (2018).

[26] Nine, M. J., Tung, T. T., Alotaibi, F., Tran, D. N. H. & Losic, D. Facile Adhesion-Tuning of Superhydrophobic Surfaces between "Lotus" and "Petal" Effect and Their Influence on Icing and Deicing Properties. *ACS Appl. Mater. Interfaces* **9,** 8393–8402 (2017).

[27] Mohamed, A. M. A., Abdullah, A. M. & Younan, N. A. Corrosion behavior of superhydrophobic surfaces: A review. *Arab. J. Chem.* **8,** 749–765 (2014).

[28] Zhou, L., Sun, G., Zhao, K., Wang, X. & Hu, A. Generalized Cassie-Baxter equation for wetting of a spherical droplet within a smooth and heterogeneous conical cavity. *Found. Appl. Phys.* **4,** 31–40 (2017).

[29] Xiao, K., Wen, L. & Jiang, L. Bioinspired superwettability materials. *Kirk-Othmer Encyclopedia of Chemical Technology*, 1–34 (2016).

[30] Young, T. An essay on the cohesion of fluids. *Philos. Trans. R. Soc. London*, 65–87 (1805).

[31] Cassie, A. B. D. . & Baxter, S. Wettability of porous surfaces. *Trans. Faraday Soc.* **40,** 546–551 (1944).

[32] Wenzel, R. Resistance of Solid Surfaces of Solid Surfaces to Wetting by Water. *Ind. Eng. Chem.* **28,** 988–994 (1936).

[33] Radwan, A. B., Abdullah, A. M. & Alnuaimi, N. A. Recent advances in corrosion resistant superhydrophobic coatings. *Corrorion Rev* **36**, 127 (2018).

[34] Hao, J. & Wang, Z. Modeling Cassie-Baxter State on Superhydrophobic Surfaces. *J. Dispers. Sci. Technol.* **37,** 1208–1213 (2015).

[35] Zhang, M., Feng, S., Wang, L. & Zheng, Y. Lotus effect in wetting and self-

cleaning. *Biotribology* **5,** 31–43 (2016).

[36] Oliveira, M. B. & Mano, J. F. Biomimetic Superhydrophobic Surfaces. *Handbook of Biomimetics and Bioinspiration*, 153–180 (2014).

[37] Barthlott, W., Neinhuis, C., Verlot, H. & Schott, C. L. Purity of the sacred lotus , or escape from contamination in biological surfaces. *Planta* **202,** 1–8 (1997).

[38] Neinhuis, C. & Barthlott, W. Characterization and Distribution of Water-repellent, Self-cleaning Plant Surfaces. *Ann. Bot.* **79,** 667–677 (1997).

[39] Feng, L., Li, S., Li, Y., Li, H., Zhang, L., Zhai, J., Song, Y., Liu, B., Jiang, L., Zhu, D. Super-Hydrophobic Surfaces: From Natural to Artificial. *Adv. Mater.* **14,** 1857–1860 (2002).

[40] Darmanin, T. Superhydrophobic and superoleophobic properties in nature. *Mater. Today* **18,** 273–285 (2015).

[41] Shin, S., Seo, J., Han, H., Kang, S., Kim, H., Lee, T., Bio-Inspired Extreme Wetting Surfaces for Biomedical Applications. *Materials* **9(2),** (2016).

[42] Darmanin, T. & Guittard, F. Recent advances in the potential applications of bioinspired superhydrophobic materials. *J. Mater. Chem. A Mater. energy Sustain.* **2,** 16319–16359 (2014).

[43] Manoharan, K. & Bhattacharya, S. Superhydrophobic surfaces review: Functional application, fabrication techniques and limitations. *J. Micromanufacturing* **2,** 59–78 (2019).

[44] Sun, W., Wang, L., Yang, Z., Li, S., Wu, T., Liu, G. Fabrication of polydimethylsiloxane-derived superhydrophobic surface on aluminium via chemical vapour deposition technique for corrosion protection. *Corros. Sci.* **128,** 176–185 (2017).

[45] Crick, C. R., Bear, J. C., Kafi, A. & Parkin, I. P. Superhydrophobic Photocatalytic Surfaces through Direct Incorporation of Titania Nanoparticles into a Polymer Matrix by Aerosol Assisted Chemical Vapor Deposition. *Adv. Mater.* **24,** 3505–3508 (2012).

[46] Tombesi, A., Li, S., Sathasivam, S., Page, K., Heale, F. L., Pettinari, C. C., Claire, J., Parkin, I. P. Aerosol-assisted chemical vapour deposition of transparent superhydrophobic film by using mixed functional alkoxysilanes. *Sci. Rep.* **9,** 7549 (2019).

[47] Lourenço, B. N., Marchioli, G., Song, W., Reis, R. L., Blitterswijk, C. A., Karperien, M., Apeldoorn, A., Mano, J. F. Wettability Influences Cell Behavior on Superhydrophobic Surfaces with Different Topographies. *Biointerphases* **7,** 46–57 (2012).

[48] Ryu, J., Kim, K., Park, J., Hwang, B. G., Ko, Y., Han, J., Seo, E., Park, Y., Lee, S. J. Nearly Perfect Durable Superhydrophobic Surfaces Fabricated by a Simple One-Step Plasma Treatment. *Sci. Rep.* **7,** 1981 (2017).

[49] Lu, Y., Xu, W., Song, J., Liu, X., Xing, Y., Sun, J. Preparation of superhydrophobic titanium surfaces via electrochemical etching and fluorosilane modification. *Appl. Surf. Sci.* **263,** 297–301 (2012).

[50] Forooshani, H. M., Aliofkhazraei, M. & Rouhaghdam, A. S. Superhydrophobic Copper Surfaces by Shot Peening and Chemical Treatment. *Surf. Rev. Lett.* **24,** 1750093-1–1750093-6 (2017).

[51] Liu, Z., Wang, H., Wang, E., Zhang, X., Yuan, R., Zhu, Y. Superhydrophobic poly(vinylidene fluoride) membranes with controllable structure and tunable wettability prepared by one-step electrospinning. *Polymer* **82,** 105–113 (2016).

[52] Bagheri, H., Aliofkhazraei, M., Forooshani, H. M. & Rouhaghdam, A. S. Electrodeposition of the hierarchical dual structured (HDS) nanocrystalline Ni surface with high water repellency and self-cleaning properties. *J. Taiwan Inst. Chem. Eng.* **80,** 883–893 (2017).

[53] Ravi, K., Lock, W., Bernard, C., Ichikawa, Y. & Ogawa, K. Fabrication of micro-/nano-structured super-hydrophobic fluorinated polymer coatings by cold-spray. *Surf. Coat. Technol.* **373,** 17–24 (2019).

[54] Hwang, H. S., Kim, N. H., Lee, S. G., Lee, D. Y., Cho, K., Park, I. Facile Fabrication of Transparent Superhydrophobic Surfaces by Spray Deposition. *ACS*

Appl. Mater. Interfaces **3,** 2179–2183 (2011).

[55] Tian, H., Wang, F., Ge, S., Ou, J., Li, W., Yu, S. A simple and Effective Way to Fabricate Mechanical Robust Superhydrophobic Surfaces. *RSC Adv.* **6,** 28563–28569 (2016).

[56] Darmanin, T., Taffi, E., Givenchy, D., Amigoni, S. & Guittard, F. Superhydrophobic Surfaces by Electrochemical Processes. *Adv. Mater.* **25,** 1378–1394 (2013).

[57] Chu, Z. & Seeger, S. Superamphiphobic surfaces. *Chem. Soc. Rev.* **43,** 2784–2798 (2014).

[58] Tian, Y., Su, B. & Jiang, L. Interfacial Material System Exhibiting Superwettability. *Adv. Mater.* **26,** 6872–6897 (2014).

[59] Deng, X., Mammen, L., Butt, H. J. & Vollmer, D. Candle soot as a template for a transparent robust superamphiphobic coating. *Science* **335,** 67–70 (2012).

[60] Costa, A. M. S., Alatorre-Meda, M., Alvarez-Lorenzo, C. & Mano, J. F. Superhydrophobic Surfaces as a Tool for the Fabrication of Hierarchical Spherical Polymeric Carriers. *Small* **11,** 3648–3652 (2015).

[61] Costa, A. M. S. & Mano, J. F. Solvent-free strategy yields size and shape-uniform capsules. *J. Am. Chem. Soc.* **139,** 1057–1060 (2017).

[62] Lima, A. C., Alvarez-Lorenzo, C. & Mano, J. F. Design Advances in Particulate Systems for Biomedical Applications. *Adv. Healthc. Mater.* **5,** 1687–1723 (2016).

[63] Song, W., Gaware, V. S., Rúnarsson, Ö. V., Másson, M. & Mano, J. F. Functionalized superhydrophobic biomimetic chitosan-based films. *Carbohydr. Polym.* **81,** 140–144 (2010).

[64] Bjørge, I. M., Costa, A. M. S., Silva, A. S., Vidal, J. P.O., Nóbrega, J. M., Mano, J. F. Tuneable spheroidal hydrogel particles for cell and drug encapsulation. *Soft Matter* **14,** 5622–5627 (2018).

[65] Erbil, H. Y., Demirel, A. L., Avci, Y. & Mert, O. Transformation of a Simple Plastic into a Superhydrophobic Surface. *Science* **299,** 1377–1380 (2013).

[66] Song, W., Veiga, D. D., Custo, C. A. & Mano, J. F. Bioinspired Degradable

Substrates with Extreme Wettability Properties. *Adv. Mater.* **21,** 1830–1834 (2009).

[67] Lima, A. C., Song, W., Blanco-fernandez, B., Alvarez-lorenzo, C. & Mano, J. F. Synthesis of Temperature-Responsive Dextran-MA/ PNIPAAm Particles for Controlled Drug Delivery Using Superhydrophobic Surfaces. *Pharm. Res.* **28,** 1294–1305 (2011).

[68] Jaiswal, M. K., Singh, K. A., Lokhande, G. & Gaharwa, A. K. Superhydrophobic states of 2D nanomaterials controlled by atomic defects can modulate cell adhesion. *Chem. Commun.* **55,** 8772–8775 (2019).

[69] Ueda, E. & Levkin, P. A. Emerging Applications of Superhydrophilic-Superhydrophobic Micropatterns. *Adv. Mater.* **25,** 1234–1247 (2013).

[70] Popova, A. A., Schillo, S. M., Demir, K., Ueda, E. & Levkin, P. A. Droplet-Array (DA) Sandwich Chip: A Versatile Platform for High-Throughput Cell Screening Based on Superhydrophobic – Superhydrophilic Micropatterning. *Adv. Mater.* **27,** 5217–5222 (2015).

[71] Popova, A. A., Depew, C., Permana, K. M., Trubitsyn, A., Peravali, R., Ángel, J., Ordiano, G., Reischl, M., Levkin, P. A. Evaluation of the Droplet-Microarray Platform for High-Throughput Screening of Suspension Cells. *SLAS Technol.* **22,** 163–175 (2017).

[72] Beyazkilic, P., Tuvshindorj, U., Yildirim, A., Elbuken, C. & Bayindir, M. Robust superhydrophilic patterning of superhydrophobic ORMOSIL surfaces for high-throughput on-chip screening applications. *RSC Adv.* **6,** 80049–80054 (2016).

[73] Xu, K., Wang, X., Ford, R. M. & Landers, J. P. Self-partitioned Droplet Array on Laser-patterned Superhydrophilic Glass Surface for Wall-less Cell arrays. *Anal. Chem.* **88,** 2652–2658 (2016).

[74] Feng, W., Li, L., Du, X., Welle, A. & Levkin, P. A. Single-Step Fabrication of High-Density Microdroplet Arrays of Low-Surface-Tension Liquids. *Adv. Mater.* **28,** 3202–3208 (2016).

[75] Popova, A. A., Demir, K., Hartanto, T. G., Schmitt, E. & Levkin, P. A. Droplet-Microarray on Superhydrophobic-Superhydrophilic Patterns for High- Throughput

Live Cell Screenings. *RSC Adv.* **6,** 38263–38276 (2016).

[76] Benz, M., Molla, M. R., Böser, A., Rosenfeld, A. & Levkin, P. A. Marrying chemistry with biology by combining on-chip solution-based combinatorial synthesis and cellular screening. *Nat. Commun.* **10,** 2879 (2019).

[77] Popova, A. A., Marcato, D., Peravali, R., Wehl, I., Schepers, U., Levkin, P. A. Fish-Microarray: A Miniaturized Platform for Single-Embryo High-Throughput Screenings. *Adv. Funct. Mater.* **28,** 1703486 (2017).

[78] Li, Y., Chen, P., Wang, Y., Yan, S., Feng, X., Du, W., Koehler, S. A., Demirci, U., Liu, B. Rapid Assembly of Heterogeneous 3D Cell Microenvironments in a Microgel Array. *Adv. Mater.* **28,** 3543–3548 (2016).

[79] Neto, A. I., Demir, K., Popova, A. A., Oliveira, M. B., Mano, J. F., Levkin, P. A. Fabrication of Hydrogel Particles of Defined Shapes Using Superhydrophobic-Hydrophilic Micropatterns. *Adv. Mater.* **28,** 7613–7619 (2016).

[80] Yang, W., Yu, H., Li, G., Wang, Y. & Liu, L. High-Throughput Fabrication and Modular Assembly of 3D Heterogeneous Microscale Tissues. *Small* **13,** 1602769 (2017).

[81] Jeon, S., Lee, J. P. & Kim, J. In situ synthesis of stimulus-responsive luminescent organic materials using a reactive inkjet printing approach. *J. Mater. Chem. C* **3,** 2732–2736 (2015).

[82] Tsotsalas, M. *et al.* Freestanding MOF Microsheets with Defined Size and Geometry Using Superhydrophobic – Superhydrophilic Arrays. *Adv. Mater. Interfaces* **3,** 1500392 (2016).

[83] Feng, W., Ueda, E. & Levkin, P. A. Droplet Microarrays: From Surface Patterning to High-throughput Applications. *Adv. Mater.* **30,** 1706111 (2018).

Chapter 2: Motivation

The present work aims to produce miniaturized freestanding (FS) membranes with controlled microscale features (i.e., size and shape) as small building blocks that could be further assembled to create large tissue constructs by bottom-up approach.

As proof-of-concept, micro-membranes will be build-up onto underlying SH-SL microarrays by the layer-by-layer (LbL) methodology. The synthetic Poly-(L-lysine) (PLL) and the natural alginate (ALG) polymers will be used as polycation and polyanion building blocks, respectively, to fabricate micro-membranes. ALG, a natural anionic biopolymer extracted from brown seaweed (*Phaeophyceae*), is particularly suitable for several biomedical applications mainly due to its similarities with ECM as well as affordable properties, including biocompatibility, non-immunogenicity and non-toxicity.[1–4] ALG will be sequentially assembled with PLL. This cationic synthetic polymer is widely used to coat tissue culture ware to improve cell attachment due to its ability to promote cell adhesion and antibacterial performance.[5–7]

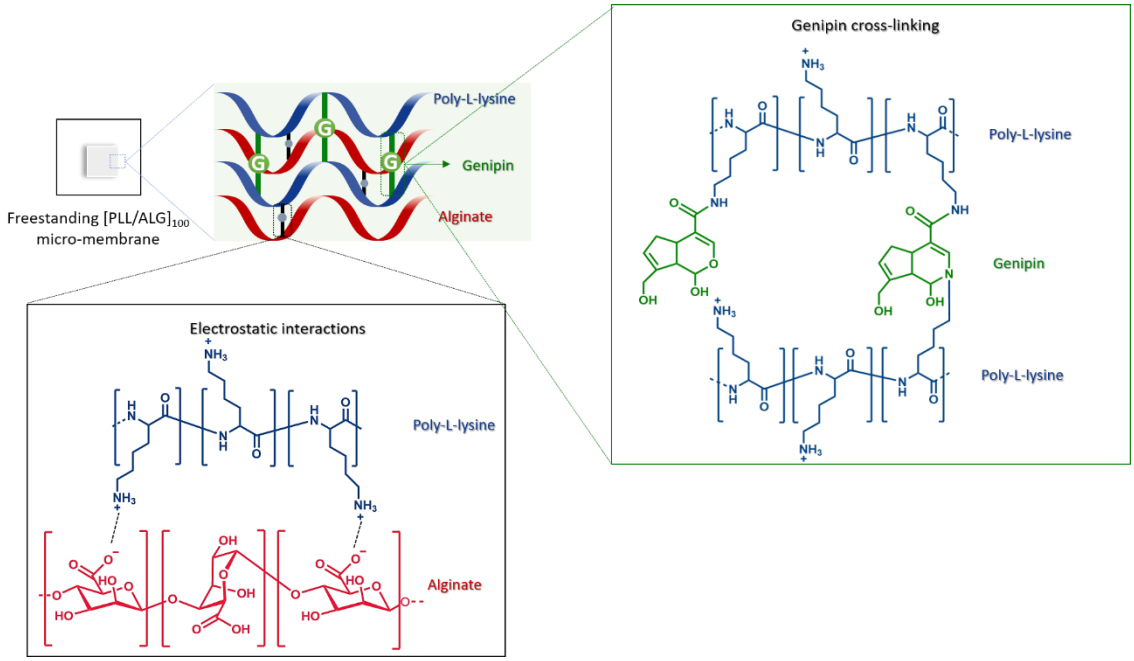

Figure 2.1 – Schematic illustration showing the multilayered rearrangements within freestanding micro-membranes, including electrostatic interactions between oppositely charged polymers (ALG and PLL) and genipin crosslinking of PLL amine groups.

A covalent crosslinking will be performed onto the micro-membranes by using genipin, in order to enhance their mechanical properties. Genipin is a naturally-derived compound extracted from *Gardenia* fruit, and it is widely used as a biocompatible crosslinker agent of polymers with amine groups. Comparing to others conventional crosslinkers such as EDC/NHS, and glutaraldehyde, genipin has shown much lower cytotoxicity, exhibiting also antioxidant and anti-inflammatory properties.[8–10] In the

particular case of hybrid multilayered membranes, since ALG does not contain amine groups, genipin crosslinker agent will give rise to semi-interpenetrating polymer networks architectures with free ALG chains entrapped inside crosslinked PLL layers, Figure 2.1.[11]

Prior to cell studies, attempts to fine-tuned biological performance of the freestanding micro-membranes will be performed by coating membrane surfaces with collagen, which is well-known to favor cell-biomaterial interactions.[12–14] In order to show the broad applicability of FS membranes for variable tissue engineering applications, different phenotypic cells will be used, namely human adipose-derived stem cells (hASCs) and human umbilical vein endothelial cells (HUVECs). Stem cells brought several advantages to the Tissue Engineering and Regenerative Medicine field, namely their ability to differentiate into multiple tissues. This is highly desirable for tissue engineering applications considering the high number of cells usually required. Particularly, hASCs are an attractive alternative compared to bone marrow MSCs, since by using a waste and abundant tissue, large quantities of stem cells can be isolated from multiple sites and by minimally invasive procedures.[15] HUVECs are members of the blood-vessel network that ensures the diffusion of essential molecules. The survival of cells within the implanted biomaterials and its integration with the host tissue is strongly dependent on nutrient and oxygen exchange, as well as waste product removal, which are provided by blood microcirculation.[16] The ability FS membranes to allow the adhesion and proliferation of cells will be evaluated *in vitro* up to 7 or 21 days, for HUVECs or hASCs, respectively. The viability of cells will be qualitatively evaluated using a calcein-AM fluorescence staining, which stains living cells in green. Additionally, a formazan-based absorbance assay will be used to quantitatively assess the metabolic activity of cells. The ability of hASCs to differentiate towards the osteogenic lineage upon 21 days of culture in osteogenic differentiation media will be also assessed. Osteogenesis will be evaluated by quantifying the activity of alkaline phosphatase (ALP) using p-nitrophenyl phosphate (pNPP) as a phosphatase substrate, and by detection of hydroxyapatite trough a fluorescence assay.

References

[1] Lee, K. Y. & Mooney, D. J. Alginate: Properties and biomedical applications. *Prog. Polym. Sci.* **37,** 106–126 (2012).

[2] Sun, J. & Tan, H. Alginate-Based Biomaterials for Regenerative Medicine Applications. *Materials* **6,** 1285–1309 (2013).

[3] Fertah, M. & Belfkira, A. Extraction and characterization of sodium alginate from Moroccan Laminaria digitata brown seaweed. *Arab. J. Chem.* **10,** S3707–S3714 (2017).

[4] Aderibigbe, B. A. & Buyana, B. Alginate in Wound Dressings. *Pharmaceutics* **10,** 42 (2018).

[5] Kosik, A., Luchowska, U. & Ś, W. Electrolyte alginate / poly-L-lysine membranes for connective tissue development. *Mater. Lett.* **184,** 104–107 (2016).

[6] Hong, D. & Yang, S. H. Cationic Polymers for Coating Living Cells. *Macromol. Res.* **26,** 1185–1192 (2018).

[7] Alkekhia, D. & Shukla, A. Influence of poly-L-lysine molecular weight on antibacterial efficacy in polymer multilayer films. *Soc. Biomater.* 1324–1339 (2019).

[8] Ghiorghita, C., Bucatariu, F. & Dragan, E. S. Materials Science & Engineering C Influence of cross-linking in loading/release applications of polyelectrolyte multilayer assemblies . A review. *Mater. Sci. Eng. C* **105,** 110050 (2019).

[9] Wang, J. *et al.* Genipin Inhibits LPS-Induced Inflammatory Response in BV2 Microglial Cells. *Neurochem. Res.* **42,** 2769–2776 (2017).

[10] Gaudière, F., Morin-grognet, S., Bidault, L., Lembre, P., Pauthe, E., Vannier, J., Atmani, H., Ladam, G. Genipin-Cross-Linked Layer-by-Layer Assemblies : Biocompatible Microenvironments To Direct Bone Cell Fate. *Biomacromolecules* **15,** 1602–1611 (2014).

[11] Silva, J. M., García, J. R., Reis, R. L., García, A. J. & Mano, J. F. Tuning cell adhesive properties via layer-by-layer assembly of chitosan and alginate. *Acta Biomater.* **51,** 279–293 (2017).

[12] Gand, A., Tabuteau, M., Chat, C., Ladam, G., Atmani, H., Tassel, P. R. V., Pauthe, E. Fibronectin-based multilayer thin films. *Colloids Surfaces B Biointerfaces* **156,** 313–319 (2017).

[13] Gong, Y., Zhu, Y., Liu, Y., Ma, Z. & Gao, C. Layer-by-layer assembly of chondroitin sulfate and collagen on aminolyzed poly (L-lactic acid) porous scaffolds to enhance their chondrogenesis. *Acta Biomater.* **3,** 677–685 (2007).

[14] Ren, K., Hu, M., Zhang, H., Li, B. Layer-by-layer assembly as a robust method to construct extracellular matrix mimic surfaces to modulate cell behavior. *Prog. Polym. Sci.* **92,** 1–34 (2019).

[15] Fraser, J. K., Wulur, I., Alfonso, Z. & Hedrick, M. H. Fat tissue: an underappreciated source of stem cells for biotechnology. *Trends Biotechnol*. **24**, 150–154 (2006).

[16] Novosel, E. C., Kleinhans, C. & Kluger, P. J. Vascularization is the key challenge in tissue engineering. *Adv. Drug Deliv. Rev*. **63**, 300–311 (2011)

Chapter 3: Article

High-throughput fabrication of freestanding micro-membranes for modular tissue engineering

High-throughput fabrication of freestanding micro-membranes for modular tissue engineering

This chapter is based on the article entitled "High-throughput fabrication of freestanding micro-membranes for modular tissue engineering"

(manuscript in preparation)

High-throughput fabrication of freestanding micro-membranes for modular tissue engineering

Flávia D. Lopes[1], Sónia G. Patrício[2#], Clara R. Correia[2#] and João F. Mano[2#]

[1] Department of Materials Engineering and Ceramics, University of Aveiro, Campus Universitário de Santiago, 3810-193, Aveiro, Portugal
[2] Department of Chemistry, CICECO – Aveiro Institute of Materials, University of Aveiro, Campus Universitário de Santiago, 3810-193, Aveiro, Portugal

[#] Corresponding Authors. E-mails: sgpatricio@ua.pt; claracorreia@ua.pt; jmano@ua.pt

Abstract

Tissue engineering (TE) has emerged as a promising alternative to regenerate injured tissues or failing organs by typically combining biomaterials, cells and biomolecules. Bottom-up or modular TE aims to mimic the complexity of native tissues by assembling repeated functional units into hierarchical engineered macro tissues. Inspired by the Lotus effect, we propose the development of miniaturized freestanding (FS) micro-membranes with spatially controlled organization through superhydrophobic-superhydrophilic (SH-SL) microarrays substrates. To achieve this purpose, alginate hydrogels were produced in SL regions as sacrificial templates for the sequential deposition of oppositely charged polyelectrolytes, namely poly-l-lysine (PLL) and alginate (ALG) biopolymers, by the layer-by-layer methodology. The successful interaction of the two biopolymers was confirmed by zeta (ζ)-potential measurements and quartz-crystal microbalance with dissipation monitoring analysis. After liquefying the sacrificial alginate microgels, the resulting detachable $[PLL/ALG]_{100}$ micro-membranes were crosslinked with genipin (GnP) in order to improve the mechanical properties, and enhance cell adhesion. Micro-membranes with variable geometries were cultured with different cells, namely squared micro-membranes were seeded with human-adipose stem cells (hASCs), and circular micro-membranes with human umbilical vein endothelial cells (HUVECs). The *in vitro* biological assays show the ability of the cross-linked $[PLL/ALG]_{100}$ FS micro-membranes to promote cell adhesion and proliferation.

Results shown that cells were able to adhere to the micro-membranes, and remained viable up to the timepoints tested, namely 7 or 21 days for HUVECs or hASCs, respectively. Additionally, both cells presented a stretched morphology visualized by F-actin staining, evidencing a successful cell-material interaction. Importantly, hASCs were able to differentiate into the osteogenic lineage, as showed by alkaline phosphatase activity and hydroxyapatite detection. Ultimately, in a proof-of-experiment, different freestanding micro-membranes cultured with HUVECs or hASCs were stacked layer-by-layer in order to achieve complex sandwich-like co-culture toward modular tissue engineering applications.

Keywords: Superhydrophobic-superhydrophilic microarrays, Layer-by-layer assembly, Freestanding micro-membranes, Modular tissue engineering

3.1. Introduction

Layer-by-layer (LbL) assembly has emerged as a promising approach to develop polymeric ultra-thin multilayered films with tailored composition and tunable properties. Such polyelectrolyte multilayered films are developed on the top of solid substrates through sequential and alternative deposition of oppositely charged polymers. When deposited on substrates with intrinsic low surface energy, these multilayered films can be easily removed without resorting to post-processing steps, thus allowing the production of freestanding (FS) membranes. Moreover, LbL is a simple, robustness and cost-effective technique that enables to assemble functional building blocks into heterogeneous multilayered structures, with finely control of the multiscale architecture, by adjusting experimental parameters such as pH, ionic strength, charge density and concentration of biopolymer species and number of sequential adsorption steps.[1–3] Polyelectrolytes assembly is mostly driven by electrostatic interactions, typically via dipping, spraying or spin coating.[4–8] Despite multilayer stability is largely governed by electrostatic interactions, others forces such as hydrogen bonding, coordination bonding, charge transfer and molecular recognition can also be involved as the driving force for the assembly process.[2,9,10]

Since the pioneering work by Decher,[11] LbL methodology has become one of the most prominent surface engineering strategies in biomedical applications, such as regenerative medicine,[12] implantable biomaterials, [13–18] drug delivery[19] and wound dressing.[20,21] For these cases, two-dimensional (2D) freestanding membranes have been explored as supportive structures for cell attachment, growth and differentiation. Recently, some strategies have been applied to the conventional LbL using flat underlying substrates in order to provide material patterned topography at the nano/micrometer scale to trigger specific cellular responses.[22,23] In a recent study,[24] nanopatterned FS membranes were generated on underlying optical media, which presents nanofeatures on their surface.[25] Biological assays shown that the presence of nanogrooved topography on the surface membranes caused the elongation of fibroblast cells along the ridges and grooves direction. Therefore, these patterned FS multilayered membranes have acted as bioinstructive substrates allowing the controlled cellular alignment, thereby playing a critical role in specific tissue regeneration, such as muscles, nerves, or blood vessels. In another work, flexible membranes containing multiple micro-reservoirs with well-defined geometric features were produced over a featured poly-dimethylsiloxane (PDMS)

template.[26] The results have shown that cells colonized preferentially in the micro-reservoirs, modulating cell behaviour in terms of migration and proliferation.

In this work, we propose a new concept of miniaturized freestanding membranes with controlled microscale features (i.e., size and shape) as small building blocks than could be further assembled into large tissue constructs toward bottom-up TE approach. For the proof-of-concept, micro-membranes were build-up onto underlying superhydrophobic-superhydrophilic (SH-SL) microarrays. These SH-SL platforms were already used to produce cell-laden microgels with well controlled geometries and sizes.[27] We endeavor to transpose this conceptual idea for a scalable manufacturing of freestanding micro-membranes. Therefore, we explore the ability of these micro-membranes to support cell adhesion and proliferation. Ultimately, in a proof-of-experiment, freestanding micro-membranes cultured with different cell phenotypes were stacked layer-by-layer in order to achieve complex sandwich-like co-culture toward modular tissue engineering applications.

3.2. Materials and Methods

3.2.1. Materials and Reagents

Glass microscope slides were purchased from Normax (Portugal). Hydrochloric acid (HCl) (37% PA), dichloromethane (99.98%), 3-(trimethoxysilyl) propyl methacrylate, 2-hydroxyethyl methacrylate (HEMA) (>98%), ethylene dimethacrylate (EDMA), 2,2-dimethoxy-2-phenylacetophenone (DMPA) (99%), cyclohexanol (99%), ethylenediaminetetraacetic acid (EDTA) (≥ 98.5%), 1H,1H,2H,2H-perfluoro-1-decanethiol (PFDT) (97%), D-(+)-gluconic acid δ-lactone (GDL) (≥99%), sodium alginate (ALG), and poly-L-lysine hydrobromide (PLL) (mol wt 30.000-70.000) were purchased from Sigma-Aldrich. 1-decanol (≥99%) was purchased from Sigma-Aldrich. 4-(dimethylamino) pyridine (99%), 4-pentyonic acid (95%) and N, N'-diisopropylcarbodiimide (99%) were purchased from Acros Organics. 2-mercaptoethanol and calcium carbonate ($CaCO_3$) were obtained from Alfa Aesar and Fluka, respectively, and sodium hydroxide (NaOH) from Eka. Genipin (GnP) was obtained from Wako and dimethyl sulfoxide (DMSO) (≥99%) was purchased from Honeywell.

3.2.2. Preparation of superhydrophobic-superhydrophilic surfaces

Superhydrophobic-superhydrophilic (SH-SL) patterned surfaces were prepared by photolithography, as previously described.[28–30] Briefly, SH-SL microarrays were prepared as stated below.

Glass slide activation, methacrylation and fluorination. Initially, glass slides were activated by immersing in 1M NaOH solution for 1 hour followed by rinsed with deionized (DI) water and immersing in 1M HCl solution for 30 min. Afterwards, glass slides were washed with DI water and dried under a nitrogen stream. Activated glass slides were modified by spreading a small amount 20% v/v ethanol solution of 3-(trimethoxysilyl)propyl methacrylate over activated glass slides. Each glass slide was covered with another activated glass slide for 30 min at room temperature (RT). Afterwards, a freshly portion of ethanolic solution was reapplied for another 30 min, and glass slides were then washed with acetone and dried under a nitrogen stream. Ultimately, glass slides were fluorinated for 3-5 hours under 50 mbar vacuum in a sealed desiccator under a trichloro (1H,1H,2H,2H-perfluorooctyl) silane atmosphere, followed by washing with acetone, and drying under nitrogen stream (see Figure S1†, supplementary information).

Polymer nanoporous film. To prepare a porous polymer layer, a polymerization mixture was prepared containing the monomer 24 wt.% HEMA, the cross-linker agent 16 wt.% EDMA, porogens by a mixture of 12 wt.% 1-decanol and 48 wt.% cyclohexanol, and the initiator 0.4 wt.% DMPA. To control the thickness of the polymer layer, two 12.5 µm thin strips of aluminum foil were applied on the corners of methacrylated glass slide. Afterwards, 80 µL of the polymerization solution were applied on top of the methacrylated glass slides, and then covered by fluorinated glass slides. Polymerization were performed by crosslinking the HEMA-EDMA polymer mixture via UV irradiation of the glass mold with 264 nm wavelength for 15 min at 12 mW/cm^2. The mold was then carefully opened using a scalpel, and the fluorinated glass slide was then removed. The polymer surface was subsequently rinsed with ethanol, and dried with a nitrogen stream. Prior to patterning, the polymerized slides were then immersed in a esterification solution containing 45 mL of dichloromethane, 56 mg of 4-(dimethylamino) pyridine, 111.6 mg of 4-pentynoic and 180 µL of *N,N'*- diisopropylcarbodiimine for 4 hours under stirring at RT followed by extensive washing with ethanol (Figure S2† (a) and (b), supplementary information).

Surface patterning. A SH pattern was created by applying 200 µL of 5% v/v solution of PFDT in acetone onto the polymer surface, followed by UV irradiation through a quartz photomask at 264 nm wavelength and 12 mW/cm^2 for 1 min. The photomask is removed, and the polymer surface is subsequently washed with acetone and dried with a nitrogen stream. A second thiol-yne reaction is then performed, leading to the modification of unreacted alkyne groups and the formation of a SH-SL pattern. The SL spots were then created by applying 200 µL of 10% v/v 2-mercaptoethanol solution in 1:1 v/v water:ethanol onto the patterned surface and irradiating the slide with 264 nm UV light and 12 mW/cm^2 for 1 min through a fluorinated quartz slide (Figure S2† (c), supplementary information). At the end, the slides were washed extensively with ethanol followed by drying with nitrogen stream.

Water contact angle measurements. Water contact angle (CA) measurements were performed on a Contact Angle System OCA and included software (Data Physics, Germany). For static contact angle measurements, digital drop shape analysis was performed on a 1 µL sessile drop of deionized water using the Laplace Young fitting routine. Each sample was evaluated at three positions with subsequent measurements at random control positions to exclude a possible bias. All measurements were performed at ambient conditions.

3.2.3. Zeta (ζ) - potential measurements of polyelectrolyte solutions

In order to assess the fabrication of PLL/ALG multilayered films via electrostatic interactions, the electrical charge of the PLL and ALG polyelectrolytes was investigated. Prior to the ζ-potential measurements, fresh solutions of PLL (1 mg.mL^{-1}) and ALG (1 mg.ml^{-1}) were prepared at pH 5.85 in ultra-pure water. The ζ-potential measurements were determined using a Zetasizer Nano ZS (Malvern Instruments, United Kingdom) at 25 °C. The measurements of each polyelectrolyte were performed in triplicate and the mean±standard deviation (SD) values were presented.

3.2.4. Quartz crystal microbalance with dissipation (QCM-D) monitoring

The build-up process of PLL/ALG multilayered films growth was evaluated by a quartz crystal microbalance with dissipation monitoring (Q-Sence, Sweden), with sensor crystals coated with gold, excited at a fundamental frequency of 5 MHz as well as at 15, 25, 35, 45 and 55 MHz corresponding to the 3rd, 5th, 7th, 9th and 11th overtones, respectively. Fresh polyelectrolyte solutions were prepared by dissolution of PLL and ALG in ultra-pure water to yield a final concentration of 1 mg.mL^{-1} at pH 5.85 adjusted

with HCl or NaOH solutions. Briefly, polyelectrolyte and washing solutions were alternatively injected into the measuring system at a constant flow rate of 50 µL.min^{-1}. The PLL solution was pumped into the system for 4 min to allow the adsorption equilibrium at the crystal surface. A rising step of 3 min with ultra-pure water was then injected in order to remove the unbound polyelectrolytes. Then, the ALG solution was pumped into the system for 4 min following a new rising step. All experiments were conducted at 25 ºC. Variations in frequency (Δf) and in dissipation (ΔD) were continuously monitored in real time until achieved the number of desired layers. Thickness measurements were performed using the Voigt viscoelastic model implemented in the QTools software (Q-Sense, version 3.1.29.619). Changes in resonant frequency and dissipation of the seventh overtone were fitted. Based on the assumed growth model, the thickness of the multilayer film after 20 cycles was estimated.

3.3. Production of micro-membranes and characterization

3.3.1. Fabrication of the hydrogel sacrificial template

The alginate hydrogel was produced by the *in situ* method, as previously described in the literature[31], with the optimization of the $CaCO_3$/GDL molar ratio to ~2.4 for the sacrificial template conditions. Herein, for the preparation of calcium alginate hydrogel, aqueous solution of ALG was prepared at 1.5% (w/v) in ultra-pure water. Afterwards, 100 µL solution of $CaCO_3$ (3.65 mg/0.100 mL) were added to 1 mL of ALG 1.5% (w/v) solution and briefly stirred. Then, 400 µL of an aqueous solution of GDL (21.78 mg/0.400 mL) was added. All fresh solutions were prepared in ultrapure water. The final solution was continuously stirred for 5 min at RT before pouring onto patterned SH-SL surface. Lastly, by standing droplet method, droplet microarray (DMA) was formed and placed (horizontally) into a stove at 37 ° C for 15 min.

3.3.2. Multilayered micro-freestanding membranes

The multilayer films were built on hydrogel sacrificial templates using freshly prepared polyelectrolyte solutions. Polyelectrolytes-based multilayered FS membranes were produced at RT via LbL assembly approach using a home-made dipping robot specially designed for the automatic fabrication of multilayers. The negatively charged hydrogel sacrificial templates were placed on top of a previously prepared patterned SH-SL surface. Then, the construct was sequentially immersed in PLL and ALG aqueous solutions (1 mg.ml^{-1}, in ultra-pure water at pH 5.8-6.0) with a rinsing step in ultra-pure water between each deposition to remove weakly adsorbed polymers. A home-made

apparatus was automatically programmed for consecutive and alternately depositions of 4 min for the polyelectrolyte solutions, and 3 min for the rinsing steps. This process was repeated until the deposition of 100 bilayers. At the end, $[PLL/ALG]_{100}$ multilayered membranes were produced by electrostatic interactions between oppositely charged polyelectrolytes. Afterwards, $[PLL/ALG]_{100}$ FS multilayered micro-membranes were obtained from the simple detachment of the sacrificial template and multilayers system by subsequent immersion in ultra-pure water and then in 100 mM EDTA solution followed to liquefy the alginate hydrogel template. Afterwards, to improve the mechanical properties, $[PLL/ALG]_{100}$ FS micro-membranes were covalent crosslinked with GnP.[32] GnP solution (1 $mg.mL^{-1}$) was prepared by dissolving GnP into DMSO:sodium acetate buffer (0.2 M NaOH, pH 5.5) mixture (1:4 ratio). The FS micro-membranes were immersed in the cross-linking solution and incubated at 37 ºC overnight. To stop the reaction, membranes were thoroughly dipped in gradual ethanol solutions until the excess of GnP was removed, and then washed and stored in DI water at RT.

3.4. Characterization

3.4.1. Attenuated total reflectance-Fourier transform infrared spectroscopy

A Bruker TENSOR 27 FTIR spectrometer fitted with a "Golden Gate" ATR module equipped with a diamond crystal was used to collect the spectra of the dried samples PLL, ALG and PLL/ALG film in the absorbance mode. All data were obtained in the spectral range of 4000-400 cm^{-1} by averaging 256 individual scans per sample at a resolution of 4 cm^{-1}. All data were processed in OPUS spectroscopy software supplied with the instrument.

3.4.2. Scanning Electron Microscopy and Energy-Dispersive X-ray Spectroscopy

The surface morphology of the samples was observed using a Hitachi S4100 (Tokyo, Japan) scanning electron microscope. Prior to the analysis, the SH-SL substrates containing the adsorbed layers, i.e. $[PLL/ALG]_{100}$ freestanding micro-membranes were fixed to the aluminum stubs by double-sided carbon conductive adhesive tape for electrical contact purposes. All samples were previously coated with a conductive layer of sputtered gold palladium. The scanning electron microscopy (SEM) micrographs were taken at an accelerating voltage of 4 kV and at different magnifications. Energy-dispersive X-ray spectroscopy (EDS, Hitachi) was also used to determine the elemental components of the top surface of the SH-SL patterned substrate. The samples were sputtered with carbon and the analysis was made at an accelerating voltage of 15 kV.

3.4.3. Optical microscopy

The optical microscope (Zeiss Stemi 508) was used to observe and magnifying the droplet microarrays (DMA) images and register them.

3.5. *In vitro* biological assays

Prior to cell studies, Gnp cross-linked $[PLL/ALG]_{100}$ FS micro-membranes were sterilized in 70% v/v ethanol for 2 h at RT. After washing with phosphate-buffered saline (PBS, Sigma-Aldrich), the FS micro-membranes were placed in cell culture slides (Invitrocell) (1 micro-membrane per well) and immersed in a collagen (Col) type I solution (from rat tail, Sigma-Aldrich) diluted in PBS (500 $\mu g.mL^{-1}$). Samples were incubated at 37°C overnight.

3.5.1. Cell culture

Human adipose-derived stem cells (hASCs) were cultured in alpha minimum essential medium (α-MEM, ThermoFisher Scientific), supplemented with 10% fetal bovine serum (FBS, ThermoFischer Scientific) and 1% antibiotic/antimycotic (ATB, ThermoFischer Scientific). Human umbilical vein endothelial cells (HUVECs) were cultured in medium 199 (M199, ThermoFisher Scientific) supplemented with 1% L-glutamax (Gibco, Life Tecnhologies), 2.5% ATB, 20% FBS and endothelial cell growth supplement (ECGs, 40 $mg.mL^{-1}$) and heparin (10 $mg.mL^{-1}$). Endothelial cells were cultured in tissue culture flasks previously treated with 0.7% gelatin (w/v, porcine skin type A, Sigma-Aldrich) for 30 min at 37 °C. hASCs and HUVECs were incubated at 37°C in a humidified air atmosphere of 5 % CO_2. Every 3-4 days, fresh medium was added.

3.5.2. $[PLL/ALG]_{100}$ FS micro-membranes seeding

At 80% of confluence, HUVECs (passage 5) and hASCs (passage 5), were washed with PBS solution, and detached using trypsin-EDTA solution (Merck) for 5 min at 37°C. Subsequently, cells were centrifuged for 5 min at 300 g to discard the supernatant. Each $[PLL/ALG]_{100}$ FS micro-membrane was seeded with 50.000 cells per cm^2. Therefore, circular FS membranes presenting a surface area of 0.07 cm^{-2} were seeded with $3.5x10^3$ HUVECs (passage 5). Squared FS micro-membranes presenting a surface area of 0.09 cm^{-2} were seeded with $4.5x10^3$ hASCs (passage 5). 3 µL of each cell suspension was placed on top of each FS micro-membranes presenting different geometries. Samples incubated at 37° in a humidified air atmosphere of 5 % CO_2. After 1.5 h, 350 µL of the appropriate culture medium was added to each well. Samples were incubated again at 37 °C in 5 % CO_2. Every 3-4 days, the cell culture medium was replaced.

3.5.3. Stacking culture

After 7 days of *in vitro* culture, HUVECs and hASCS seeded in circular and square shaped FS micro-membranes, respectively, were staked by placing one circular micro-membrane on top of one square micro-membrane. Stacked samples were incubated at 37 °C in a humidified air of 5 % CO_2. A 1:1 ratio of each specific cell culture media was used.

3.5.4. Calcein-AM and DAPI–phalloidin fluorescence assays

To evaluate the cellular viability of hASCs and HUVECs seeded on PLL/ALG FS micro-membranes (1 micro-membrane per well, in duplicate), a calcein fluorescence assay was performed. Briefly, at 1, 3 and 7 days of culture, cell culture medium was removed and 300 µL of PBS containing 0.6 µL of calcein-AM (1 $mg.mL^{-1}$, Invitrogen) was added to each well. Samples were then incubated at 37 ºC for 15 min protected from light. Afterwards, samples were washed with PBS and immediately visualized in the dark by fluorescence microscopy (Axioimage RZ1M, Zeiss, Germany).

In order to observe the cell nucleus and F-actin filaments, *4,6*-Diaminidino-*2*-phenylindole-dilactate (DAPI, Sigma-Aldrich) and phalloidin tetramethylrhodamine *B* isothiocyanate (phalloidin, Sigma-Aldrich, USA) fluorescent dyes were used, respectively. HUVECs were visualized at 1, 3 and 7 days of culture, and hASCs 1, 3, 7, 14 and 21 days of culture. At each timepoint, cell culture medium was removed, and 10% v/v of formalin (Biosciences) was added to each well for 45 min at RT. Afterwards, cells were permeabilized with 0.1% v/v Triton-X (Sigma Aldrich) for 5 min at RT. Upon PBS washing, 300 µL of 1 mL of PBS containing 7.5 µL phalloidin (50 $\mu g.mL^{-1}$, Flash Phalloidin Red 594, Biolegend) was added to each sample. After 45 min at RT, the samples were washed with PBS and counterstained with DAPI in a PBS solution of 300 µL with 0.3 µL DAPI (1 $mg.mL^{-1}$, Sigma-Aldrich). After 5 min at RT and protected from light, the samples were washed with PBS and visualized in the dark by fluorescence microscopy (Axio Imager 2, Zeiss). Cells nuclei appeared bright blue and F-actin filaments appeared bright red due to DAPI and phalloidin dyes, respectively.

3.5.5. Metabolic activity colorimetric assay

The cytotoxicity of $[PLL/ALG]_{100}$ FS micro-membranes seeded with hASCs or HUVECs was tested using an MTS colorimetric assay. This metabolic activity assay is based on the bio reduction ability of mitochondrial dehydrogenase enzymes present in viable cells to convert the *3*-(*4,5*-dimethylthiazol-*2*-yl)-*5*-(*3*-carboxymethoxyphenyl)-*2*-(*4*-

sulphofenyl)-2H-tetrazolium (MTS) compound into a cell culture soluble brown formazan product. Briefly, FS micro-membranes were placed in cell culture slide (Invitrocell) (1 micro-membrane per well in triplicate) and incubated for 1, 3 and 7 days at 37 ºC and in a humidified 5% CO_2 atmosphere. The MTS assay was performed protected from light. The culture medium was removed and 300 µL of PBS containing MTS solution with a dilution ratio of 1:5 was added to each well. Samples were then incubated in the dark at 37 ºC and 5% CO_2. After 4 h, the contents of each well were transferred to eppendorf tubes (in triplicate) followed by centrifugation at 450 g for 5 min. Then, 100 µL of each eppendorf were transferred to a 96-well plate. The amount of formazan product was measured by absorbance at a wavelength of 490 nm using a multiwall spectrophotometer (Synergy HT, Bio-TEK).

3.5.6. DNA and alkaline phosphatase activity quantification assays

The ability of FS micro-membranes to support the proliferation of hASCs and HUVECs was tested by DNA quantification assay. Quantification of total DNA was determined after cell lysis, according to the manufacturer's description (Quant-iTTM PicoGreen® dsDNA assay kit, Life Technologies). Briefly, at different pre-determined culture periods, samples (1 membrane per well in triplicate) were washed with PBS and subsequently suspended in 300 L of ultra-pure sterile water. Upon mixing, the contents were transferred to eppendorf tubes. After 1 h in a 37 ºC shaking water bath, samples were frozen at -80ºC overnight or until use. Samples were defrosted and used according to the specifications of the kit. After transferring each solution to a 96-well white opaque plate (in duplicate), the plate was incubated at RT protected from light for 10 min. Fluorescence was read at excitation of 485/20 nm and emission of 528/20 nm using a microplate reader (Gen 5 2.01, Synergy HT, Biotek). The standard curve for DNA analysis was generated with provided DNA from the assay kit.

The activity of alkaline phosphatase (ALP) of hASCs cultured in the FS membranes was determined. Briefly, a substrate solution (pH 9.8) was prepared by dissolving *4*-nitrophenylphosphate disodium salt hexahydrate (0.2% w/v, Sigma-Aldrich) in diethanolamine (1 M, Sigma-Aldrich). Each sample (20 µL, in duplicate) was mixed with the prepared substrate solution (60 µL). After 1h at 37 ºC protected from light, the reaction was stopped (80 µL) with NaOH (2 M) and EDTA (0.2 mM). A standard curve with a range of concentrations (0, 0.05, 0.10 and 0.15 in triplicate) was prepared by diluting *4*-nitrophenol solution (10 mM, Sigma-Aldrich) in the stop solution. Absorbance was read

at 405 nm in a microplate reader (Gen 5 2.01, Synergy HT, Biotek). Results were normalized with the DNA quantification data.

3.5.7. Mineralization fluorescent assay

At 21 days of hASCs culture, the presence of hydroxyapatite (HA) crystals was assessed using the OsteoImage™ Mineralisation Assay kit (Lonza) according to the manufacturer's instructions. Then, samples were counterstained with DAPI (1:1000 in PBS, 1 $mg.mL^{-1}$, ThermoFisher Scientific) for 5 min at RT, and visualized by fluorescence microscopy (Axio Imager 2, Zeiss).

3.5.8. Statistical analysis

Statistical analysis was performed using one-way analysis of variance (ANOVA) with Tukey's post-hoc test. p-values <0.05 were considered statistically significant (****p<0.0001; ***p<0.001; **p<0.01; *p<0.05). All results are presented as mean ± standard deviation of at least three independent experiments.

3.6. Results and Discussion

3.6.1. Production and characterization of SH-SL microarrays

To produce the SH–SL microarrays, a nanoporous HEMA–EDMA film was formed onto a glass slide, followed by modifying the polymer surface with alkyne groups through a standard esterification procedure (Figure S1†, supplementary information). Afterwards, a SH pattern with two different geometries, namely circles and squares were formed by functionalizing the surface with 1H,1H,2H,2H-perfluorodecanethiol (PFDT) through photo-click thiol-yne reaction and by applying a corresponding quartz photomask. After this patterning step, the non-irradiated areas still comprise reactive alkyne groups for a secondary chemical modification. This one corresponds to another thiol-yne reaction with 2-mercaptoethanol, forming superhydrophobic-superhydrophilic patterns (Figure S2†).[29] Applying the discontinuous dewetting method, the extreme difference in wettability between the SL spots and SH borders leads to the formation of a high-density array of completely separated microdroplets (Figure 3.1), where water was spontaneously removed from the barriers, but filled SL regions. As previously related, as soon as the nanoporous SL areas becomes wet, these regions become transparent due to the reduced light scattering caused by matched refractive indexes.[27] The analysis of CAs has confirmed the extreme difference in wettability. SH barriers possessed CAs of 179.9 ±

0.6°, while the SL areas showed CAs of 25.5 ± 0.2º. This latter value is above 10º, meaning that wettable regions are hydrophilic rather than superhydrophilic.

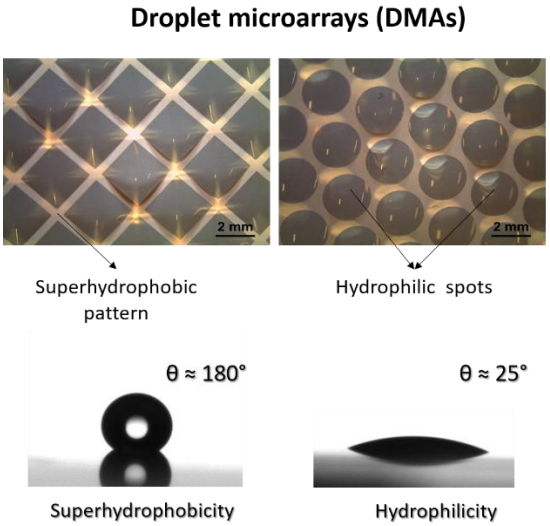

Figure 3.1 – Optical images of the formation of droplet microarrays (DMAs) with circular and square geometries. A large droplet of water was applied onto the patterned surface. Upon applying a slight tilt to the slide, the droplets roll off the surface spontaneously by discontinuous dewetting.

The surface morphology and chemical composition of the SH-SL patterned surfaces produced was also analyzed by SEM and EDS. The SH-SL polymer layer obtained shown a thickness of 12 μm corresponding to the thickness of the aluminum foil used as spacer. Additionally, the surface have presented small size of pores that was important for achieving transparency of the wetted polymer film (see Figure S3†, supplementary information). EDS mapping of SH-SL surfaces have revealed the presence of the key elements of the thiols used for the formation of either superhydrophobic or superhydrophilic areas (Figure 3.2). In this sense, SH barriers have shown enriched F borders (red color) due to the presence of PFDT, which has a long carbon chain and is therefore responsible for the highly hydrophobic characteristic of the produced patterned surfaces. Furthermore, the Sulphur element from 2-mercaptoethanol (short carbon chain thiol) is mainly located on the SL spots. These results corroborated the well-succeed thiol-yne click reactions for the production of SH-SL droplet microarrays.

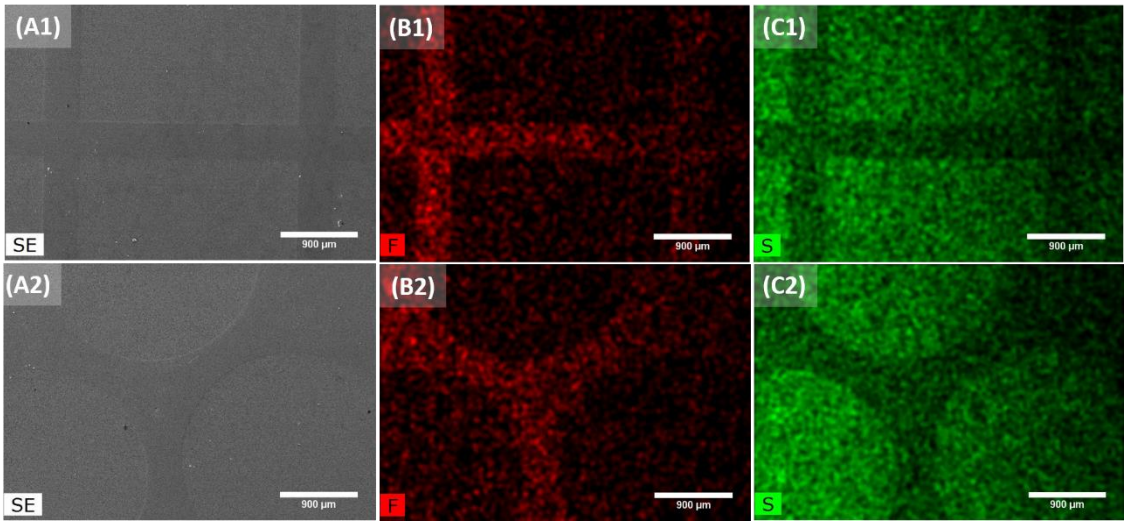

Figure 3.2 – SEM (SE) images of a SH-SL patterned surface with square (A1) and circular (A2) geometries. EDS mapping (B1-B2) showing the red SH barriers enriched in fluor (F), and the green SL areas (C1-C2) in sulphur (S). Scale bar: 900 µm.

3.6.2. Build-up of PLL/ALG multilayered films

The LbL approaches are mainly based on electrostatic interactions.[8] In this sense, prior to QCM-D monitoring, the ζ-potential of the different polyelectrolyte solutions was measured (Figure 3.3 A) under working conditions. As expected, at pH 5.85 PLL presented a positive charge (+55.3 ± 1.3 mV) while the ALG solution exhibit negative electrical charge (-65.8 ± 0.1 mV). These results confirm the cationic and anionic nature of PLL and ALG, respectively, which allowed the successfully build-up of multilayered self-assembled films by electrostatic interactions. Afterwards, the buildup of PLL/ALG multilayered films, through the sequential adsorption of the oppositely charged polyelectrolytes, was followed in situ by QCM-D monitoring. Figure 3.3 B shows the variations of the normalized frequency ($\Delta f_v / v$) and dissipation (ΔD) of the 7th overtone corresponding to the deposition of 20 bilayers of PLL/ALG, onto the gold-coated quartz crystal substrates. The curves represent the state of frequency and dissipation after each material deposition which can be distinguished by the stepwise decrease in frequency, and increase in dissipation. The decrease of the normalized frequency in each deposition step indicates that the polymeric mass was adsorbed onto the gold-coated quartz crystals representing the successful deposition of polyelectrolytes. Regarding the increasing in the energy dissipation after each polyelectrolyte layer deposition, this indicates the non-rigid behavior as well as the viscoelastic nature of the materials absorbed above the crystal substrates.

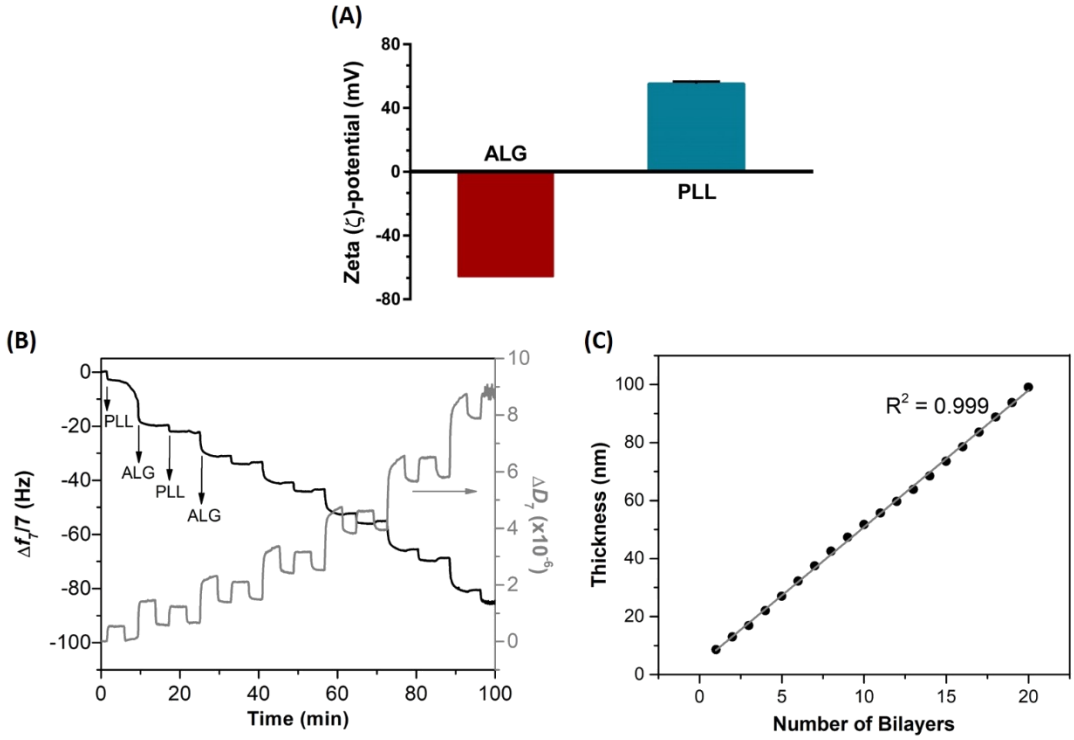

Figure 3.3 – (A) ζ-potential analysis of poly-l-lysine (PLL) and alginate (ALG). (B) Build-up assembly assessment of PLL and ALG up to 20 deposition bilayers in ultra-pure water. Results correspond to the quartz-crystal microbalance with dissipation monitoring (QCM-D) of normalized frequency ($\Delta f_o/v$) and dissipation (ΔD) variations correspondent to the PLL deposition and the ALG deposition, obtained at the seventh overtone as a function of time. (C) Cumulative thickness evolution of the PLL/ALG polymeric film as a function of the number of bilayers of polyelectrolytes deposition. Thickness measurements were estimated using the Voigt viscoelastic model.

Moreover, the QCM-D data were also used to estimate the thickness variations of the multilayered films along with the film building, as shown in Figure 3.3 C. Assuming a viscoelastic film, the polyelectrolyte layers were modeled as an elastic component in parallel with a viscous component – the Voigt-based Viscoelastic Model.[20,33] As a result, a linear growth model was observed during the construction of twenty bilayers. The analysis of the cumulative thickness evolution also allows to predict the film growth mode, suggesting the formation of a homogeneous film. Therefore, we assumed that this behavior will be maintained for the deposition of the other *n* bilayers, and the overall thickness for the [PLL/ALG]$_n$ FS micro-membranes could be extrapolated.

3.7. Fabrication and characterization of micro-freestanding membranes

QCM-D experiments confirmed the successful electrostatic interaction between the selected polyelectrolytes. Afterwards, freestanding micro-membranes were fabricated by using a homemade dipping robot. In order to allow the membrane detachment from the microarray platform, hydrogel sacrificial templates were produced onto SH-SL micro-patterns.

3.7.1. Manufacture of microgels by the *in-situ* method as a sacrificial template to produce freestanding membranes

ALG can easily forms hydrogels through the replacement of the sodium cation with divalent cations (such as Ca^{2+}) that act as ionic crosslinkers. ALG hydrogels crosslinked with Ca^{2+} present a structure known as "the egg-box model", in which Ca^{2+} cooperatively interact with blocks of G monomers of the polymer forming tightly bound interactions.[34] Slow gelation led to the formation of uniform gel structures with greater mechanical integrity. In order to control the gelation rate, ALG was associated with $CaCO_3$ and GDL. $CaCO_3$ was used since it has a very low solubility in ultra-pure water. This allows the uniform distribution of ALG before gelation occurs. Then, the suspension is acidified by adding GDL, and the hydrolysis lead to the slow release of Ca^{2+} ions from the $CaCO_3$, thus initiating the gelation process. Lastly, in order to increase the gelation, the SH-SL patterned substrate with hydrogel sacrificial templates was incubated at 37 ºC.[31,34–36] Calcium alginate hydrogels were produced *in situ* on the SH-SL patterned substrates with controlled geometric shape and volume by formation of a DMA using the standing droplet method (Figure S3†, supplementary information). When an aqueous solution is rolled along the surface, the extreme wettability contrast of SL spots on an SH background leads to the formation of a high-density array of separated microdroplets.

Afterwards, a homemade dipping robot was used to fabricate the $[PLL/ALG]_{100}$ FS micro-membranes over hydrogel sacrificial templates, through consecutive and sequential adsorption of PLL and ALG by immersing them in the respective polyelectrolyte intercalated with washing steps at RT (Figure 3.4 A).

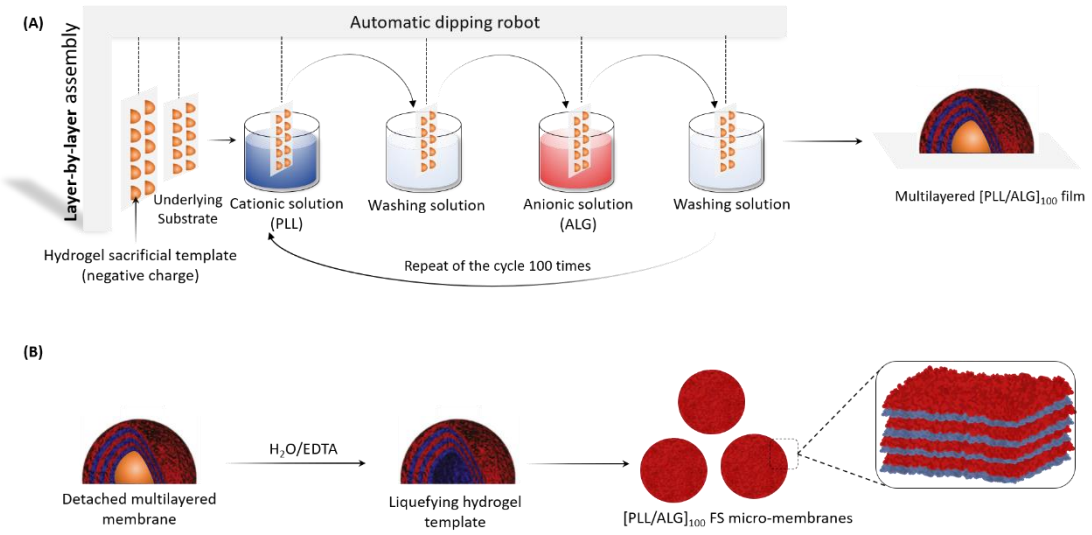

Figure 3.4 – (A) Schematic representation of the construction of multilayered membranes by the LbL technique using the dipping robot onto sacrificial templates to produce robust freestanding (FS) $[PLL/ALG]_{100}$ membranes by electrostatic interactions. (B) Detachment process of $[PLL/ALG]_{100}$ FS micro-membranes. First, the substrates are immersed in ultra-pure water, and then the hydrogel and the micro-membranes were immersed in 100 mM EDTA solution.

At the end, $[PLL/ALG]_{100}$ FS micro-membranes with square and circular geometries (3mm of dimension) were obtained from the simple detachment of the sacrificial template and multilayers system in ultra-pure water followed by immersion in EDTA solution. Calcium alginate hydrogels are destabilized in the presence of Ca^{2+} chelators agents, such as EDTA, which accelerate the swelling of the alginate matrix due to the dissociation of the gel matrix. Under these conditions, EDTA chelates Ca^{2+} ions, thus liquefying the hydrogel (see Figure 3.4 B).[37] Thus, we were able to obtain FS multilayered micro-membranes by LbL technique using hydrogels as sacrificial template onto SH-SL patterned surfaces.

SEM images of the non-crosslinked $[PLL/ALG]_{100}$ FS micro-membranes produced by LbL technique over SH-SL patterned surfaces are shown in Figure 3.5 (A-B). SEM images show that multilayered FS micro-membranes are able to preserve their geometric shape, although they were slightly smaller due to the dehydration effect with ethanol. Previous displacement of the formed films was also observed (Figure 3.5 B), demonstrating the facile detachment of the membranes. The morphology of the freestanding micro-membranes was also analyzed by SEM. $[PLL/ALG]_{100}$ surface micro-membrane has shown a quite homogeneous morphology, presenting some surface roughness (Figure 3.5 C). The cross-section of the $[PLL/ALG]_{100}$ FS micro-membranes (Figure 3.5 D), also presented an homogeneous and stratified morphology. Using the Image J software, the thickness of multilayered FS micro-membranes was measured,

presenting 4.99 ± 0.05 µm, which is 10 magnitude higher than the estimated thickness by the Voigt model of the QCM-D results. A possible reason is the influence of the deposition substrate, which quasi-3D onto the microarray platform increasing the amount of adsorbed polymer and, thus increasing the thickness of the micro-membrane.

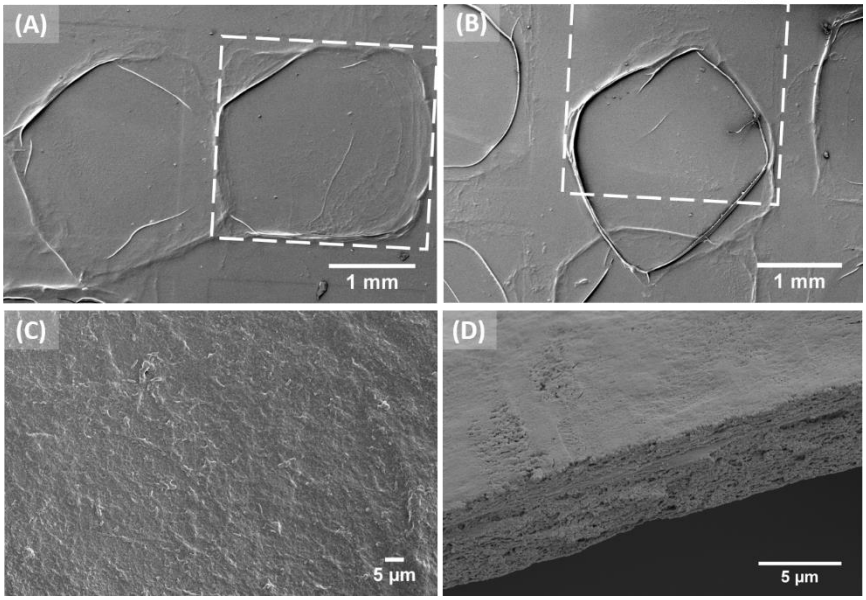

Figure 3.5 – SEM images of the [PLL/ALG] micro-membranes produced over SH-SL patterned surfaces (A-B). (C) SEM image of the morphology correspondent at $[PLL/ALG]_{100}$ freestanding multilayered micro-membrane. The cross-section of the $[PLL/ALG]_{100}$ micro-membrane is presented in (D). Scale bars represents 1 mm (A,B), and 5 µm (C,D).

The FTIR technique provides information about the chemical composition of the micro-membranes. ATR-FTIR measurements were performed on dry samples to examine the characteristic bands of PLL and ALG individual polymers as well as of the FS multilayered membranes. The results are illustrated in Figure 3.6. The FTIR spectrum of ALG reveals well-defined absorption bands at ≈ 1595 and 1405 cm^{-1}, which are assigned to the asymmetric and symmetric stretching vibrations of the carboxylic group, respectively. Moreover, it also shows peaks in the range 950–1200 cm^{-1}, which are due to the skeletal vibrations of the carbohydrate ring.[38,39] The spectrum of PLL molecule evidence two peaks at 1646 (amide I) and 1540 cm^{-1} (amide II), indicating that the PLL polymer existed primarily in the α-helix conformation. The amide I band (range from 1700 to 1600 cm^{-1}) correspond, mainly, to the stretching vibrations of the C=O and also the C–N bonds of the amide group, whereas the amide II band (range from 1600 to 1500 cm^{-1}) arise from the stretching and bending vibrations of the N–H bonds.[39]

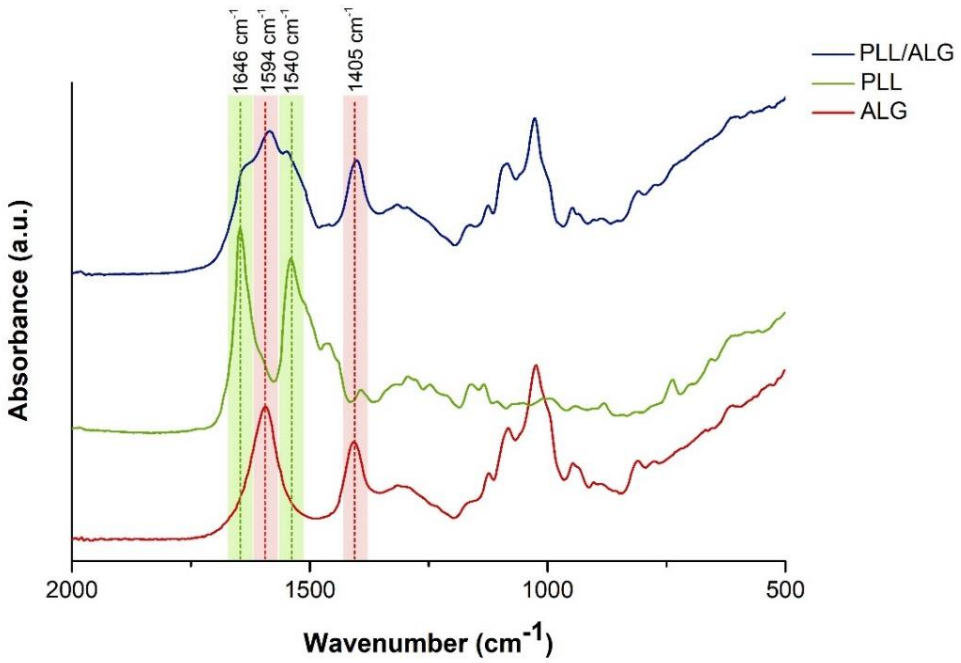

Figure 3.6 – ATR-FTIR absorbance spectra of the PLL/ALG multilayered membranes and their compounds.

The ATR-FTIR absorbance spectrum of the PLL/ALG membrane confirms that ALG and PLL compounds are presented in the multilayered membrane. The analysis of spectrum of PLL/ALG membrane reveal the presence of peaks at ≈ 1594 and 1405 cm^{-1} that are also identified in the spectrum of the ALG biopolymer. Moreover, the spectrum of the multilayered film also shows two peaks near 1646 and 1540 cm^{-1}, which are characteristic of the amide I and II bands of PLL, respectively.

Prior to cell studies, FS micro-membranes were covalently crosslinked with genipin (GnP) a naturally non-cytotoxic compound that is able to spontaneously react with amino group, forming a crosslinked network through polymerization.[32,40] Typically, the reaction of GnP with primary amines originates a deep blue coloration, which color intensity can be correlated with crosslinking degree. Figure 3.7 shows FS micro-membranes photographs with different geometric shapes (circles and squares) before and after GnP crosslinking. The initial colorless micro-membranes turned dark green in an extended period of time reaction, suggesting a high crosslinking degree of amine groups in FS micro-membranes. We hypothesize that the formation of semi-interpenetrated crosslinking networks could modulate the stiffness and roughness of the membranes, thus tuning cell adhesion.

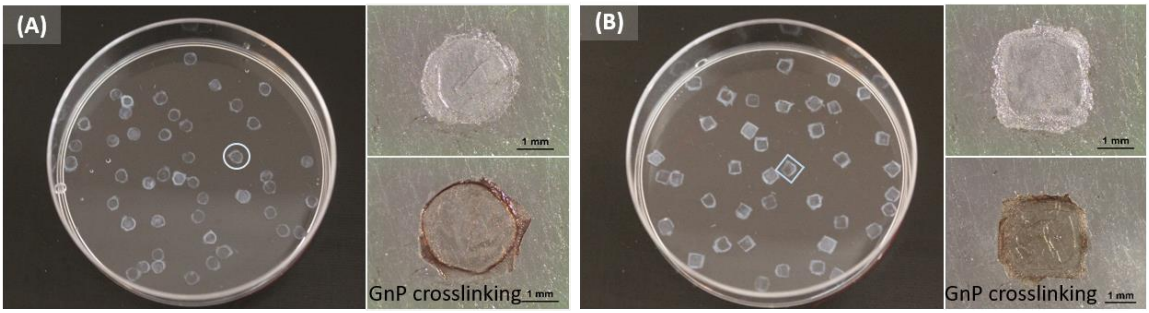

Figure 3.7 – Detachable $[PLL/ALG]_{100}$ micro-membranes with (A) circular and (B) square geometry, the correspondent crosslinked micro-membranes with genipin (brown membranes). Scale bar represents 1mm.

3.8. *In vitro* biological assays

After crosslinking with genipin, $[PLL/ALG]_{100}$ micro-membrane surfaces were still subjected to a post-treatment with collagen. It should be mentioned that, after detachment from the underlying sacrificial template, the bottom (PLL) and top (ALG) layers become undistinguished, providing different surface properties for cell adhesion. In this sense, prior to cell seeding, the multilayered membrane surface was coated with collagen. To study the collagen coating effect onto PLL (bottom) and ALG (top) layered membrane surface, a QCM-D in situ collagen adsorption experiment was performed (Figure 3.8).

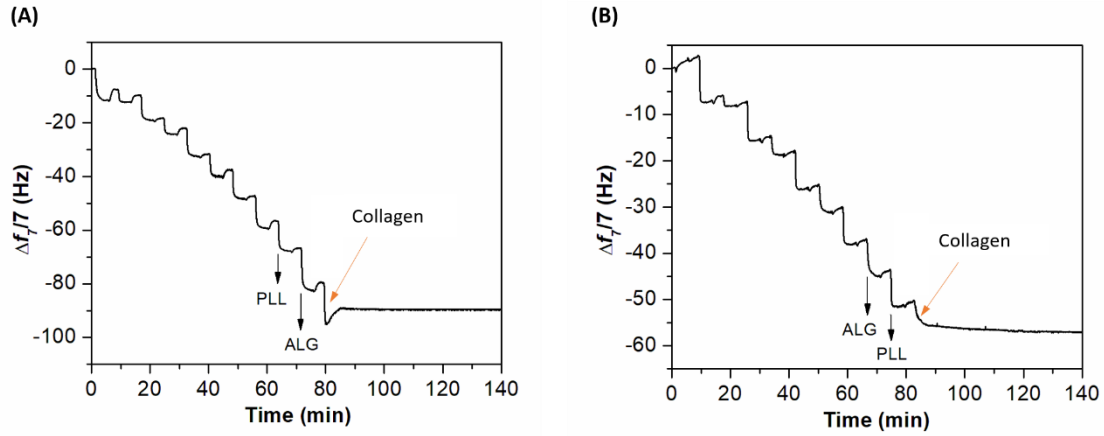

Figure 3.8 – Monitoring collagen adsorption over (A) $[PLL/ALG]_5$ and (B) $[ALG/PLL]_5$ multilayered assembly.

Two different types of films were produced onto gold-coated quartz sensors: $[PLL/ALG]_5$ and $[ALG/PLL]_5$, following by collagen adsorption onto the outermost ALG and PLL layers, respectively. As expected, upon collagen addition, a decrease in frequency was observed for the $[PLL/ALG]_5$ film (Figure 3.8 A), confirming the successful electrostatic adsorption of collagen on ALG outer layer. Interestingly, a slight frequency decrease was also noticed for $[ALG/PLL]_5$ film, even when the outer layer is positively charged. In this case, we hypothesized that collagen adsorption onto PLL layer could occur through

hydrogen bonds. Therefore, collagen coating onto FS micro-membranes would be well succeeded independently the top layer composition of membranes (ALG or PLL).

The use of adult stem cells in TE strategies presents a viable alternative for the regeneration of human tissues. Amongst the different multipotent sources, hASCs has been shown to exhibit the triple multilineage differentiation potential, and they can be easily obtained from liposuction waste.[41–44] Controlling the differentiation fate of stem cells represents a challenging task requiring a three-dimensional (3D) environment, which is commonly achieved by micromass culture[45,46] or, for example, using scaffolds composed by natural and/or synthetic polymers[47] combined with a finely tuned supply of growth factors. HUVECs represent a widely used source of primary endothelial cells for *in vitro* studies of angiogenesis. Moreover, HUVECs are relatively easy to isolate avoiding contamination by other cell types, and umbilical cord is readily available as discarded biological waste after the child's born.[48] Endothelial cells constitute the inner lining of blood vessels which control the nutrients and oxygen exchanges, as well as waste product, for the survival of cells, and subsequently integration of biomaterials with the host tissue. Additionally, the highly vasculature of the native bone also delivers the calcium and phosphate indispensable for the mineralization/osteogenesis process.[48,49]

Thus, the endothelial cells are used to form vascular network serving as a "template" for bone mineral deposition promoting vascularization in bone tissue engineering. In this sense, inspired by the local interactions at the molecular level from the co-existence of stem and vascular cells in the native environment of bone, stem (hASCs) and endothelial (HUVECs), and the potential of combining osteogenic cells with endothelial cells to achieve *in vitro* pre-vascularization within scaffold constructs[50], hASCs and HUVECs were used for evaluating the cellular viability of the biomaterial/device developed.

Therefore, *in vitro* biological assays were performed with HUVECs or hASCs in order to observe the interaction of $[PLL/ALG]_{100}$ FS micro-membranes with two cell phenotypes. As showed in the calcein assay (Figure 3.9 A) at days 1, 3 and 7, hASCs were viable, thus emitting a fluorescent green light. DAPI-Phalloidin fluorescence assay (Figure 3.9 D and I) at 1 day shows that both cells presented stretched F-actin filaments and a normal morphology.

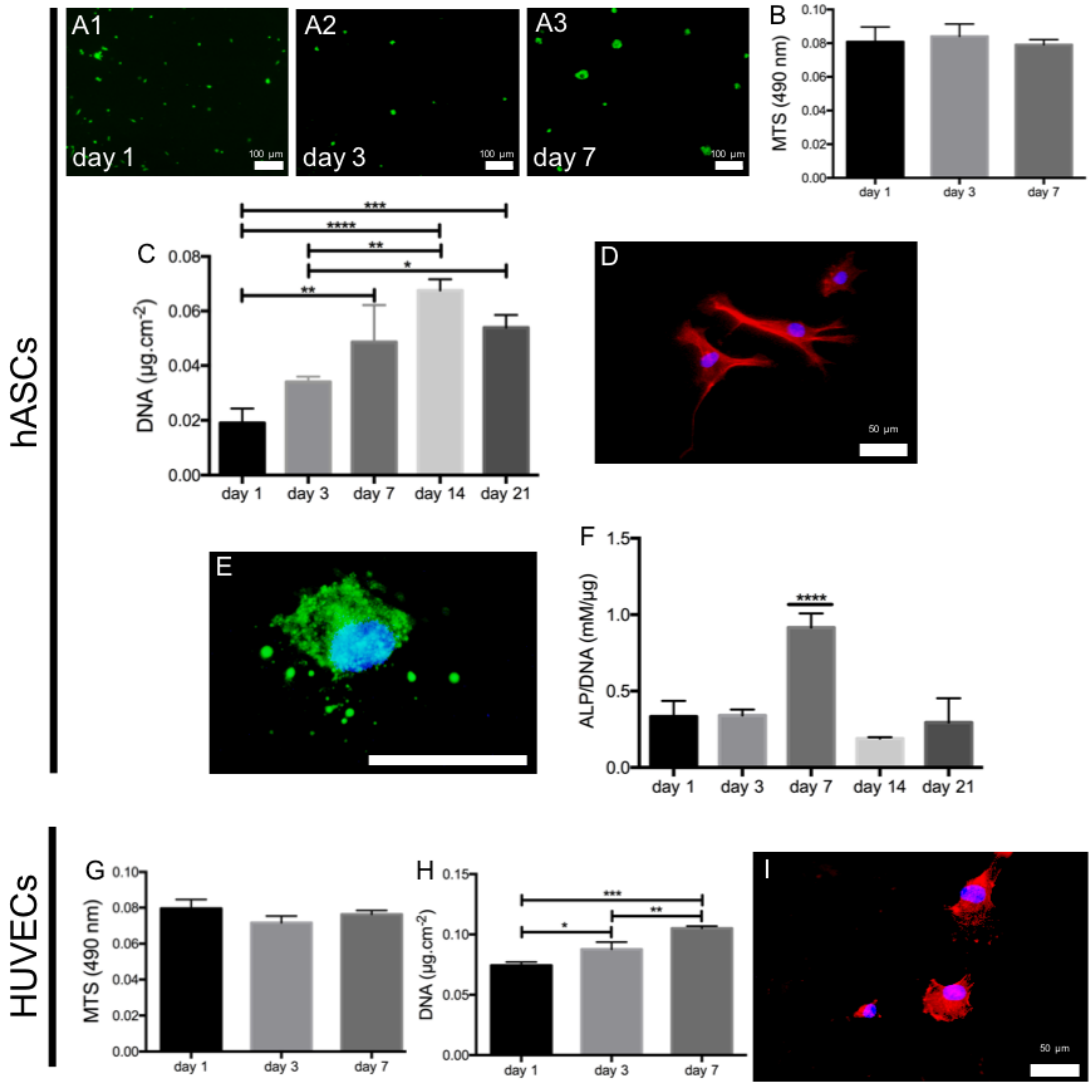

*Figure 3.9 – (A1-A3) Calcein fluorescence assay of hASCs at 1, 3 and 7 days of culture. Living cells were stained by calcein (green). (B) MTS colorimetric assay of hASCs at 1, 3, and 7 days of culture. (C) Cell proliferation evaluation by DNA quantification of hASCs up to 21 days of culture. (D) DAPI-Phalloidin fluorescence assay of hASCs seeded in FS micro-membranes at 1 day of culture. Cells nuclei were stained in blue by DAPI and F-actin filaments in red by phalloidin. Scale bar is 50 µm. (E) Mineralization fluorescence assay. Hydroxyapatite is stained in green using the commercially available Osteoimage kit, and cells nuclei in blue by DAPI. Scale bar is 50 µm. (F) Alkaline phosphatase (ALP) activity quantification of hASCs up to 21 days of culture. For statistical analysis of the ALP only the peak at day 7 is marked because all timepoints compared to day 7 show this difference. (G) MTS colorimetric assay of HUVECs at 1, 3, and 7 days of culture. (H) Cell proliferation evaluation by DNA quantification of HUVECs up to 7 days of culture. (I) DAPI-Phalloidin fluorescence assay of hASCs seeded in FS micro-membranes at 1 day of culture. Cells nuclei were stained in blue by DAPI and F-actin filaments in red by phalloidin. Scale bar is 50 µm. *p<0.05 values were considered statistically significant (**p<0.01, ***p<0.001, and ****p<0.0001).*

The metabolic activity of seeded hASCs and HUVECs onto cross-linked $[PLL/ALG]_{100}$ FS micro-membranes was assessed at different time points (1,3 and 7 days) through a MTS colorimetric assay (Figures 3.9 B and G). The results show a similar metabolic activity up to the 7 days of *in vitro* culture, without significant differences between the cell phenotypes (hASCs and HUVECs). This can be an indication that cross-linked FS micro-membranes provide a suitable substrate for cellular growth without cytotoxic

effects for cells. In Figure 3.9 E, it is possible to observe the presence of hydroxyapatite, an indicator of the osteogenic differentiation of hASCs. The ability of cells to proliferate in the crosslinked $[PLL/ALG]_{100}$ FS micro-membranes was evaluated by DNA quantification. As showed in Figure 3.9 B, hASCs showed an increased DNA content up to 14 days of culture, evidencing their ability to proliferate. At day 21 a slight decrease could be noticed. However, between day 7, 14 and 21 days any statistically significant differences could be detected. Additionally, the ability of hASCs to differentiate into the osteogenic lineage was assessed by ALP quantification. ALP is an enzyme secreted by active osteoblasts, and is responsible for the cleavage of pyrophosphate ions, which are inhibitors of the formation of hydroxyapatite crystals. The hydrolysis reaction results in the saturation of the extracellular fluid with orthophosphates that induce mineralization.[51] Increased levels of ALP activity are thus correlated with enhanced osteogenic differentiation.[52] As showed in Figure 3.9 F, the peak of ALP activity was achieved at day 7. The DNA quantification of HUVECs (Figure 3.9 H), shows that cells were able to proliferate up to the 7 days of in vitro culture.

Ultimately, in a proof-of-experiment, FS micro-membranes (square and circular geometries) cultured with different cell phenotypes were stacked in a sandwich-like structure providing a wider range of programmability to experimental design (e.g. geometry, growth area and surface modification) compared to traditional 2D cell culture platforms.[53] Cells were seeded onto FS micro-membranes before the assembly of the stacked micro-membranes. After 7 days of culture in each specific cell culture media, square and circular FS micro-membranes with hASCs and HUVECs, respectively, were assembly in a sandwich-like structure. For that, the circular micro-membrane was placed on top the square micro-membrane (Figure 3.10 A). When the culture medium (1: 1 ratio of each specific cell culture medium) was added, the stacked micro membranes remained overlapped. This evidences the successful self-assembly of the micro-membranes. After 7 and 14 days in co-culture, the stacked micro-membranes were visualized by fluorescence microscopy. However, the results proved were inconclusive, due to GnP autofluorescence (Figure 3.10 B).

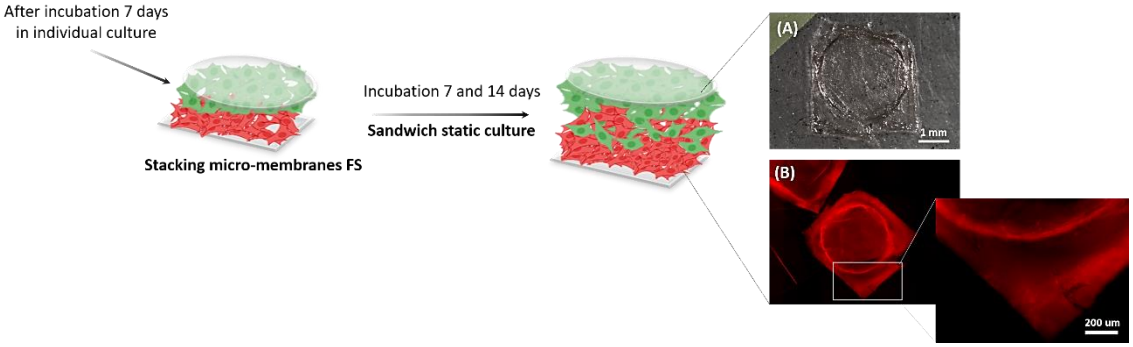

Figure 3.10 – Stacking of micro-membranes in a sandwich-like structure. (A) Optical image of stacked micro-membranes after 14 days. (B) Fluorescence microscopy images highlighting GnP autofluorescence.

3.9. Conclusions

For the first time, a new concept of miniaturized freestanding membranes based on SH-SL droplet microarrays was developed to be used as small building blocks for modular tissue engineering. Biological *in vitro* assays carried out with two different cell phenotypes (hASCs and HUVECs) have shown the ability of these FS micro-membranes to support cell adhesion and proliferation. Our first attempt to produce sandwich-like co-culture microstructures requires further improvements to be used as an effective methodology for modular tissue engineering.

Acknowledgements

This work was supported by the European Research Council grant agreement ERC-2014-ADG-669858 (project ATLAS), by the Operational Program Competitiveness and Internalization, in its FEDER component, and national funds (OE), through FCT – Fundação para a Ciência e Tecnologia I.P., in the scope of the project MIMETIc (PTDC/BTM-MAT/31210/2017) and of the project CICECO-Aveiro Institute of Materials (UID/CTM/50011/2019),. This work was still supported by the Marine Biotechnology ERA-NET project "BLUETEETH" (ERA-MBT/0002/2015), funded under the European Commission's Seventh Framework Programme (Grant Agreement No. 604814).

References

[1] Xiao, F., Pagliaro, M., Xu, Y. & Liu, B. Layer-by-layer assembly of versatile nanoarchitectures with diverse dimensionality: a new perspective for rational construction of multilayer assemblies. *R. Soc. Chem.* **45,** (2016).

[2] Mao, Z., Yu, S. & Gao, C. Bioactive and Spatially Organized LbL Films. in *Layer-by-Layer Films for Biomedical Applications* 79–102 (Wiley-VHC Verlag GmbH & Co, 2015).

[3] Zhang, S., Xing, M. & Li, B. Biomimetic Layer-by-Layer Self-Assembly of Nanofilms, Nanocoatings, and 3D Scaffolds for Tissue Engineering. *Int. J. Mol. Sci.* **19,** 1641 (2018).

[4] Zhang, X., Xu, Y., Zhang, X., Wu, H., Shen, J., Chen, R. Progress on the layer-by-layer assembly of multilayered polymer composites: Strategy , structural control and applications. *Prog. Polym. Sci.* **89,** 76–107 (2019).

[5] Borges, J., Sousa, M. P., Cinar, G., Caridade, S. G., Guler, M. O., Mano, J. F. Nanoengineering Hybrid Supramolecular Multilayered Biomaterials Using Polysaccharides and Self-Assembling Peptide Amphiphiles. *Adv. Funct. Mater.* **27,** 1605122 (2017).

[6] Gribova, V., Auzely-velty, R. & Picart, C. Polyelectrolyte Multilayer Assemblies on Materials Surfaces : From Cell Adhesion to Tissue Engineering. *Chem. Mater.* **24,** 854–869 (2012).

[7] Richardson, J. J., Cui, J., Bjo, M., Braunger, J. A., Ejima, H., Caruso, F. Innovation in Layer-by-Layer Assembly. *Chem. Rev.* **116,** 14828–14867 (2016).

[8] Borges, J. & Mano, J. F. Molecular interactions driving the layer-by-layer assembly of multilayers. *Chem. Rev.* **114,** 8883–8942 (2014).

[9] Richardson, J. J., Björnmalm, M. & Caruso, F. Technology-driven layer-by-layer assembly of nanofilms. *Science* **348,** (2015).

[10] Costa, R. R. & Mano, J. F. Polyelectrolyte multilayered assemblies in biomedical technologies. *Chem. Soc. Rev.* **43,** 3453–3479 (2014).

[11] Decher, G. & Schmitt, J. Buildup of ultrathin multilayer films by a self-assembly process: III. Consecutively alternating adsorption of anionic and cationic polyelectrolytes on charged surfaces. 831–835 (1992).

[12] Ren, K., Hu, H., Zhang, H., Li, B. Layer-by-layer assembly as a robust method to construct extracellular matrix mimic surfaces to modulate cell behavior. *Prog. Polym. Sci.* **92,** 1–34 (2019).

[13] Gentile, P., Carmagnola, I., Nardo, T. & Chiono, V. Layer-by-layer assembly for biomedical applications in the last decade. *Nanotechnology* **26,** 422001 (2015).

[14] Kulikouskaya, V. I., Pinchuk, S. V., Hileuskaya, K. S., Kraskouski, A. N., Vasilevich, I. B., Matievski, K. A., Agabekov, V. E., Volotovski, I. D. Layer-by-layer buildup of polysaccharide-containing films : Physico-chemical properties and mesenchymal stem cells adhesion. *J. Biomed. Mater. Res. Part A* **106,** 2093–2104 (2018).

[15] Zeng, J. & Matsusaki, M. Layer-by-layer assembly of nanofilms to control cell functions. *Polym. Chem.* **10,** 2960–2974 (2019).

[16] Correia, C. R., Pirraco, R. P., Cerqueira, M. T., Marques, A. P., Reis, R. L., Mano, J. F. Semipermeable Capsules Wrapping a Multifunctional and Self-regulated Co-culture Microenvironment for Osteogenic Differentiation. *Sci. Rep.* **6,** (2016).

[17] Kozlovskaya, V., Chen, J., Zavgorodnya, O., Hasan, M. B. & Kharlampieva, E. Multilayer Hydrogel Capsules of Interpenetrated Network for Encapsulation of Small Molecules. *Langmuir* **34,** 11832–11842 (2018).

[18] Oliveira, M. B., Hatami, J. & Mano, J. F. Coating Strategies Using Layer-by-layer Deposition for Cell Encapsulation. *Chem. - An Asian J.* **11,** 1753–1764 (2016).

[19] Habibi, N. Pastorino, L., Babolmorad, G., Ruggiero, C., Guda, T., Ong, J. Polyelectrolyte multilayers and capsules : S-layer functionalization for improving stability and biocompatibility. *J. Drug Deliv. Sci. Technol.* **38,** 1–8 (2017).

[20] Sousa, M. P. *et al.* Bioinspired multilayer membranes as potential adhesive patches for skin wound healing. *Biomater. Sci.* **6,** 1962–1975 (2018).

[21] Martins, N. I., Neto, A. I., Correia, T. R., Miguel, S. P., Matsusaki, M., Correia, I. J., Mano, J. F. Multilayered Membranes with Tuned Well Arrays to Be Used as Regenerative Patches. *Acta Biomater.* **57,** 313–323 (2017).

[22] Nikkhah, M., Edalat, F., Manoucheri, S. & Khademhosseini, A. Engineering microscale topographies to control the cell-substrate interface. *Biomaterials* **33,** 5230–5246 (2012).

[23] Sousa, M. P., Arab-tehrany, E., Cleymand, F. & Mano, J. F. Surface Micro- and Nanoengineering: Applications of Layer-by-Layer Technology as a Versatile Tool to Control Cellular Behavior. *Small* **15,** 1901228 (2019).

[24] Sousa, M. P., Caridade, S. G. & Mano, J. F. Control of Cell Alignment and Morphology by Redesigning ECM-Mimetic Nanotopography on Multilayer Membranes. *Adv. Mater.* **6,** (2017).

[25] Anene-Nzelu, C. G., Choudhury, D., Li, H., Fraiszudeen, A., Peh, K. Y., Toh, Y. C., Ng, S. H., Leo, H. L., Yu, H. Scalable cell alignment on optical media substrates. *Biomaterials* **34,** 5078–5087 (2013).

[26] Martins, N. I., Sousa, M. P., Custódio, C. A., Pinto, V. C., Sousa, J., Minas, G., Cleymand, F., Mano, J. F. Multilayered membranes with tuned well arrays to be used as regenerative patches. *Acta Biomater.* **57,** 313–323 (2017).

[27] Neto, A. I., Demir, K., Popova, A. A., Oliveira, M. B., Mano, J. F., Levkin, P. A. Fabrication of Hydrogel Particles of Defined Shapes Using Superhydrophobic-Hydrophilic Micropatterns. *Adv. Mater.* **28,** 7613–7619 (2016).

[28] Ueda, E., Geyer, F. L., Nedashkivska, V. & Levkin, P. A. DropletMicroarray: Facile formation of arrays of microdroplets and hydrogel micropads for cell screening applications. *Lab Chip* **12,** 5218–5224 (2012).

[29] Feng, W., Li, L., Ueda, E., Li, J., Heißler, S., Welle, A., Trapp, O., Levkin, P. A. Surface Patterning via Thiol-Yne Click Chemistry: An Extremely Fast and Versatile Approach to Superhydrophilic-Superhydrophobic Micropatterns. *Adv. Mater. Interfaces* **1,** 1400269 (2014).

[30] Geyer, F. L., Ueda, E., Liebel, U., Grau, N. & Levkin, P. A. Superhydrophobic–Superhydrophilic Micropatterning: Towards Genome-on-a-Chip Cell Microarrays. *Angew. Chem. Int. Ed.* **50,** 8424–8427 (2011).

[31] Bidarra, S. J., Barrias, C. C. & Granja, P. L. Injectable alginate hydrogels for cell delivery in tissue engineering. *Acta Biomater.* **10,** 1646–1662 (2014).

[32] Silva, J. M., García, J. R., Reis, R. L., García, A. J. & Mano, J. F. Tuning cell adhesive properties via layer-by-layer assembly of chitosan and alginate. *Acta Biomater.* **51,** 279–293 (2017).

[33] Dunér, G., Thormann, E. & De, A. Quartz Crystal Microbalance with Dissipation (QCM-D) studies of the viscoelastic response from a continuously growing grafted polyelectrolyte layer. *J. Colloid Interface Sci.* **408,** 229–234 (2013).

[34] Simó, G., Fernández-fernández, E. & Vila-crespo, J. Research progress in coating techniques of alginate gel polymer for cell encapsulation Research progress in coating techniques of alginate gel polymer for cell encapsulation. *Carbohydr. Polym.* **170,** 1–14 (2017).

[35] Kuo, C. K. & Ma, P. X. Ionically crosslinked alginate hydrogels as scaffolds for tissue engineering : Part 1 . Structure , gelation rate and mechanical properties. *Biomaterials* **22,** 511–521 (2001).

[36] Szekalska, M., B, A. P., N, E. S., Ciosek, P. & Winnicka, K. Alginate : Current Use and Future Perspectives in Pharmaceutical and Biomedical Applications. *Intermational J. Polym. Sci.* (2016). doi:10.1155/2016/7697031

[37] Ching, S. H., Bansal, N. & Bhandari, B. Alginate gel particles – A review of production techniques and physical properties. *Crit. Rev. Food Sci. Nutr.* **57,** 1133–1152 (2017).

[38] Sartori, C., Finch, D. S. & Ralph, B. Determination of the cation content of alginate thin films by FTi.r. spectroscopy. *Polymer* **38,** 43–51 (1997).

[39] Tam, S. K. *et al.* Physicochemical model of alginate – poly-L-lysine microcapsules defined at the micrometric / nanometric scale using ATR-FTIR, XPS, and ToF-SIMS. *Biomaterials* **26,** 6950–6961 (2005).

[40] Hillberg, A. L., Holmes, C. A. & Tabrizian, M. Biomaterials Effect of genipin cross-linking on the cellular adhesion properties of layer-by-layer assembled polyelectrolyte films. *Biomaterials* **30,** 4463–4470 (2009).

[41] Aust, L., Devlin, B., Foster, S. J., Halvorsen, Y. D. C., Hicok, K., Laney, T. Yield of human adipose-derived adult stem cells from liposuction aspirates. *Cytotherapy* **6,** 7–14 (2004).

[42] Mahmoudifar, N. & Doran, P. M. Mesenchymal Stem Cells Derived from Human Adipose Tissue. in *Cartilage Tissue Engineering: Methods and Protocols, Methods in Molecular Biology* **1340,** 53–64 (Springer Science+Business Media New York, 2015).

[43] Estes, B. T., Diekman, B. O., Gimble, J. M. & Guilak, F. Isolation of adipose-derived stem cells and their induction to a chondrogenic phenotype. *Nat. Protoc.* **5,** 1294–1311 (2010).

[44] Bielli, A., Scioli, G., Gentile, P., Cervelli, V. & Orlandi, A. Adipose-derived stem cells in cartilage regeneration : current perspectives. *Regen. Med.* **11,** 693–703 (2016).

[45] Fayol, D. *et al.* Use of Magnetic Forces to Promote Stem Cell Aggregation During Differentiation , and Cartilage Tissue Modeling. *Adv. Mater.* **25,** 2611–2616 (2013).

[46] Georgi, N., Blitterswijk, C. A. van & Karperien, M. Mesenchymal Stromal/Stem Cell–or Chondrocyte-Seeded Microcarriers as Building Blocks for Cartilage Tissue Engineering. *Tissue Eng. Part A* **20,** 2513–2523 (2014).

[47] Nooeaid, P., Schulze-tanzil, G. & Boccaccini, A. R. Stratified Scaffolds for Osteochondral Tissue Engineering. *Cartilage Tissue Engineering: Methods and Protocols, Methods in Molecular Biology* **1340,** 191–200 (2015).

[48] Kocherova, I., Bryja, A., Mozdziak, P., Volponi, A. A., Piotrowska-kempisty, H., Antosik, P., Dyszkiewicz-konwi, M. Human Umbilical Vein Endothelial Cells (HUVECs) Co-Culture with Osteogenic Cells : From Molecular Communication to Engineering Prevascularised Bone Grafts. *J. Clin. Med.* **8,** 1602 (2019).

[49] Costa-Almeida, R., Granja, P. L., Soares, R. & Guerreiro, S. G. Cellular Strategies to Promote Vascularisation in Tissue Engineering Applications. *Eur. Cells Mater.* **28,** 51–67 (2014).

[50] Deegan, A. J., Hendrikson, W. J., El Haj, A. J. & Rowkema, J. Regulation of endothelial cell arrangements within hMSC e HUVEC co-cultured aggregates. *Biomed. J.* **42,** 166–177 (2019).

[51] Niu, X., Ye, K., Wang, L., Lin, Y. & Du, D. A review on emerging principles and strategies for colorimetric and fluorescent detection of alkaline phosphatase activity. *Anal. Chim. Acta* **1086,** 29–45 (2019).

[52] Straalen, J. P. Van, Sanders, E., Prummel, M. F. & Sanders, G. T. B. Bone-alkaline phosphatase as indicator of bone formation. *Clin. Chim. Acta* **201,** 27–34 (1991).

[53] Veliz, D. S., Zhang, H. & Toivakka, M. Stacking up: a new approach for cell culture studies. *Biomater. Sci.* **7,** 3249–3257 (2019).

Supplementary information

High-throughput fabrication of freestanding micro-membranes for modular tissue engineering

Flávia D. Lopes[1], Sónia G. Patrício[2#], Clara R. Correia[2#] and João F. Mano[2#]

[1] Department of Materials Engineering and Ceramics, University of Aveiro, Campus Universitário de Santiago, 3810-193, Aveiro, Portugal
[2] Department of Chemistry, CICECO – Aveiro Institute of Materials, University of Aveiro, Campus Universitário de Santiago, 3810-193, Aveiro, Portugal

[#] Corresponding Authors. E-mails: sgpatricio@ua.pt; claracorreia@ua.pt; jmano@ua.pt

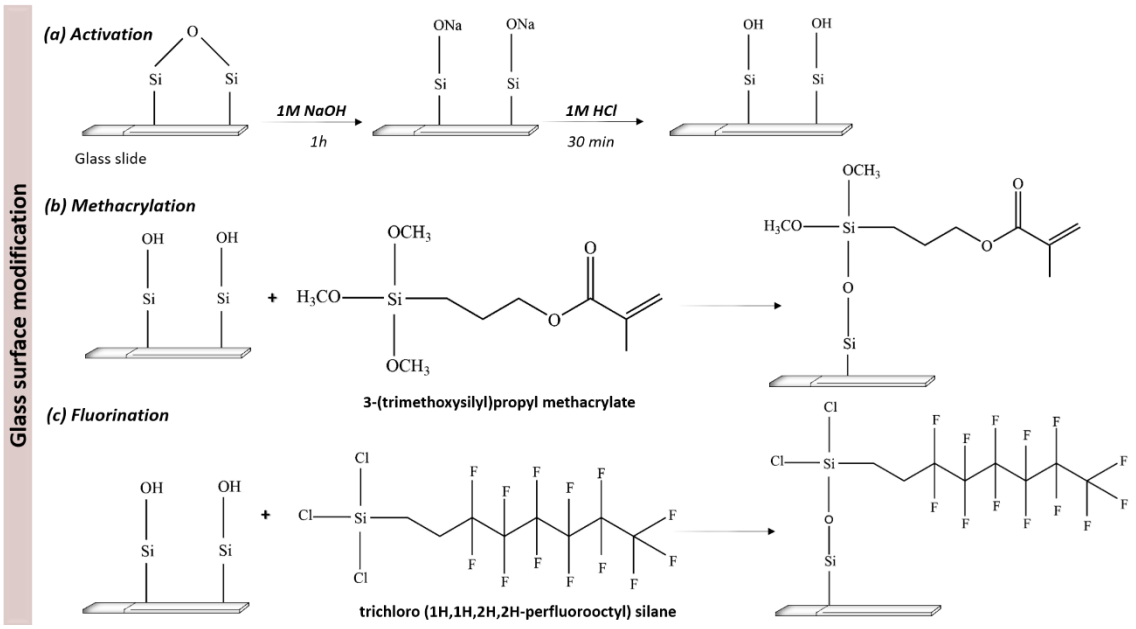

Figure S1† - Scheme of the (a) activation, (b) methacrylation and (c) fluorination of the glass slides.

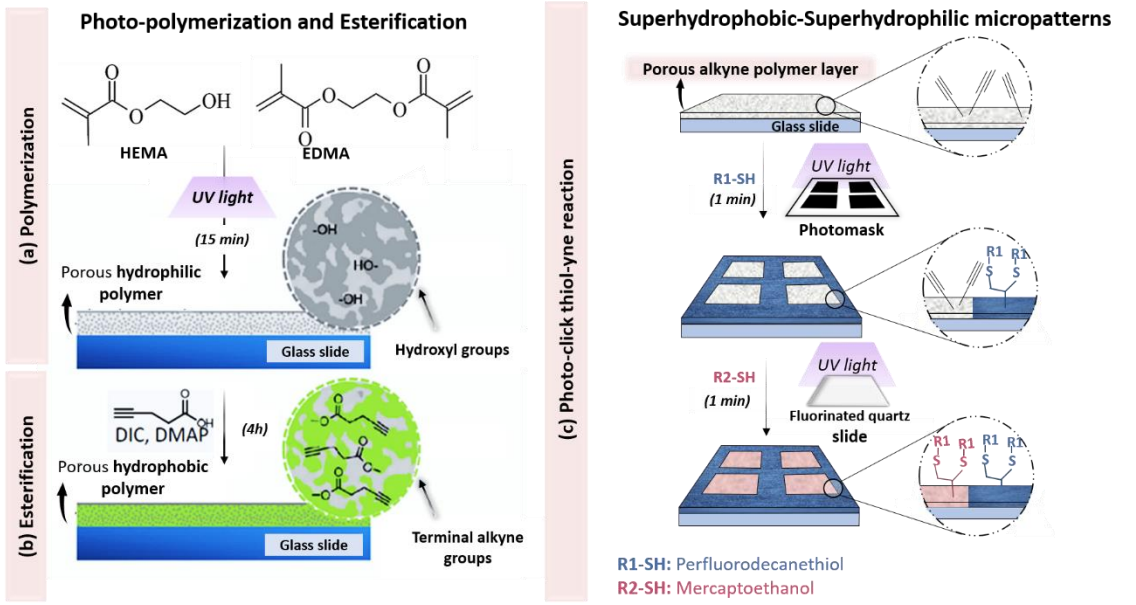

Figure S2† - Scheme of the fabrication of (a) a superhydrophilic (SL) nanoporous film (HEMA-EDMA) and (b) a superhydrophobic (SH) polymer layer by polymerization and esterification reactions, respectively; and (c) thiol-yne photo-click reaction for creating SH-SL micropatterns using the alkyne-modified porous polymer layer as a substrate. R1-SH and R2-SH correspond to hydrophobic and hydrophilic thiols, respectively.

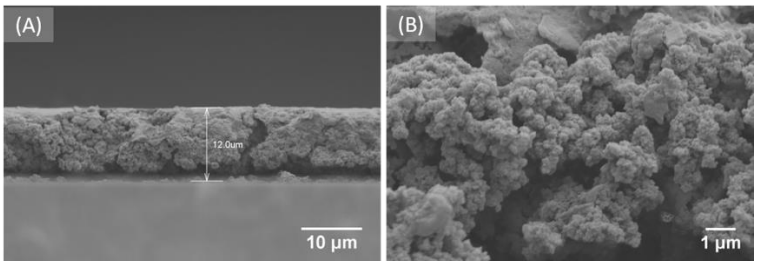

Figure S3† - SEM images of nanoporous film. (A) – surface thickness of 12 µm and (B) – surface porosity. Scale bar represents 10 µm and 1 µm, respectively.

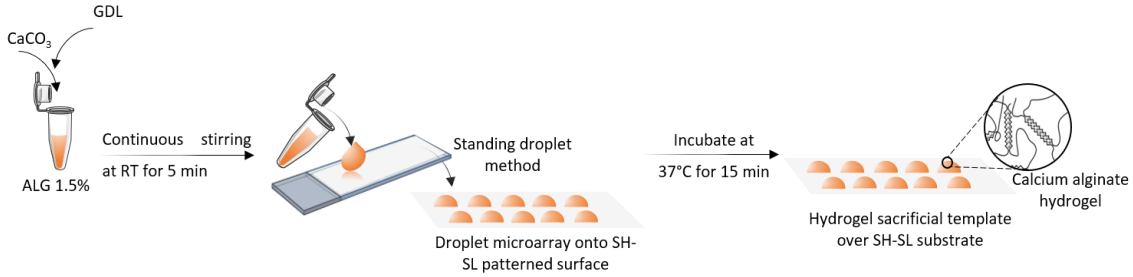

Figure S4† - Schematic diagram of the formation of calcium alginate hydrogel as a sacrificial template over SH-SL micropatterned substrate.

Chapter 4: General Conclusions and Future Perspectives

In tissue engineering (TE), the restricted availability of donor tissues and organs for transplantation has fostered the quest of alternative therapeutic strategies to repair or replace damaged human tissues. Nowadays, TE approaches holds the promise of creating engineered biological tissues in order to overcome the drawbacks between the donor and the transplantation needs. Various cell types, biomaterials and stimulatory signals, either alone or in combination, have been explored for biomedical applications, namely to mimic the architecture, complexity and/or functionality of native tissues. Bottom-up or modular approaches focuses on fabricating multiple tissue building blocks with specific microstructural features enabling to mimic native tissue architectures. Modular building blocks once created can be assembled into larger engineered tissue by generating repeated functional units (biomaterial-cells) through different assembly strategies (e.g. stacking).
Among the technologies to produce modular units, SH-SL microarrays emerged as scalable platforms to develop modular microscale units with well controlled shape and size, which can be further assembled to create engineered macrotissues.
Herein, the main goal was to create sophisticated multilayered FS micro-membranes by using SH-SL microarrays that might find great applicability for the regeneration of tissues as cell microcarriers. To achieve this purpose, alginate hydrogels were formed in situ in SL areas which served as sacrificial template for the production of thin multilayered membranes. Quasi-3D freestanding multilayered micro-membranes with different patterned features to control cellular spatial organization for specific tissue regeneration strategies, were developed from PLL and ALG biopolymers by LbL immersive assembly and, characterized by several techniques. Then, the mechanical stability of $[PLL/ALG]_{100}$ micro-membranes was improved with covalent crosslinking with GnP, and collagen type I coating was used to promote cell attachment. Inspired by the local interactions at the molecular level from the co-existence of stem and vascular cells in the native environment of bone, stem (hASCs) and endothelial (HUVECs) cells were seeded in square and circular micro-membranes, respectively. Biological assays were performed, and overall results show that the cross-linked $[PLL/ALG]_{100}$ FS micro-membranes developed were able to support cell adhesion up to 7 or 21 days, for HUVECs or hASCs, respectively.
Our proof-of-concept (see Figure 4.1 A) suggest that these FS micro-membranes may eventually be assembled into larger structures by modular tissue engineering, mimicking the complex hierarchical organization of native tissues. Thus, this novel strategy of multilayered FS micro-membranes at microscale developed promise to have versatile and tunable models in biomedical applications as an effective methodology to assemble

micro-membranes (modular unit blocks) into larger structures through stacking. The stacking configuration can comprise FS micro-membranes with different geometric shapes and containing different cells (according to desired application, e.g. bone regeneration, vasculature or neuronal networks). Such versatile features might find great application for modular tissue engineering, aiding in the recreation of the complex microstructural features of native tissues. For that, we envision that it is required further improvements in the micro-membranes proposed, such as an increased number of bilayers and a different crosslinking method, for example with EDC/NHS, in order to enhance cell-interactions.

Considering the future perspectives, an innovate approach is envisioned which consists in applying a dynamic culture system that mimics the dynamic environment of native tissues. For that, FS micro-membranes seeded with cells will be cultured using bioreactors (see Figure 4.1 B). We hypothesize that in such dynamic culture environment, aggregates of cells and FS micro-membranes can be formed. Further studies and otpimizations/modifications are needed to exploit the potential of the presented device. However, the simplistic approach proposed together with the ease of production and scalable of the FS micro-membranes to a large volume make it a potentially useful and feasible new approach for the study of co-cultures of different cells phenotypes and to mimic in vivo environments.

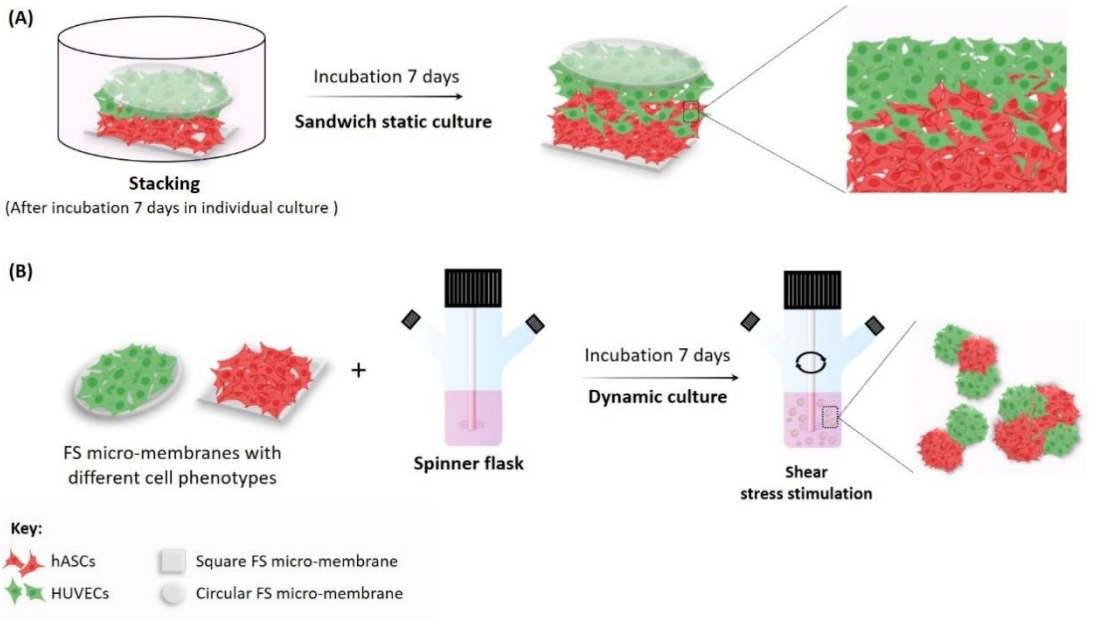

Figure 4.1 – (A) Proof-of-concept: stacking the FS $[PLL/ALG]_{100}$ micro-membranes as modular units to creating a larger structure to mimic hierarchical organization of native tissues. (B) Bio-assembly of micro-membranes in dynamic environment.